Regional Patterns and Climatic Drivers of Snow Cover Duration

in the Taurus Mountains from 2000-2019

Chrysanthos Farmakis

Delft University of Technology

TU Delft

Regional Patterns and Climatic Drivers of Snow Cover Duration

in the Taurus Mountains from 2000-2019

by

Chrysanthos Farmakis

to obtain the degree of Master of Science
at the Delft University of Technology,
to be defended publicly on Monday, October 18, 2022 at 14:45 AM.

Student number: 5346746
Project duration: January 11, 2022 – October 18, 2022
Thesis committee: Dr. Markus Hrachowitz, Associate Professor, TU Delft, supervisor
Dr. Stef Lhermitte, Assistant Professor, TU Delft

An electronic version of this thesis is available at http://repository.tudelft.nl/.

TU Delft

Abstract

Seasonal snow is the major water resource of more than a billion people around the world. In a plethora of regions in the Northern Hemisphere, agricultural, industrial, and drinking water supply are highly dependent on seasonal snow. In addition, the melting of seasonal snow regulates the magnitude and timing of high and low flows, controls the length of the growing season, and determines land surface warming via the albedo feedback. The aim of the study is to quantify the local and regional dynamics of snow cover in the Taurus mountain range and to identify the main climatic drivers responsible for the detected snow cover variability. A data-driven approach based on satellite observations is followed for the systematic analysis of large-scale snow cover in the region of interest. Compared to various remote-sensing snow cover studies that focus either on small/catchment scales, with limited spatial context, or on continental scales that cannot provide detailed insights into a specific region, this study investigates local and regional spatial patterns and temporal dynamics of snow cover across a specific mountain range of interest. The objectives of this study are: (a) to quantify the snow cover temporal variability in the different sub-regions of the Taurus mountain range, (b) to analyze the trends and to identify the regional differences, and (c) to examine the sensitivity of annual snow cover duration to inter-annual climatic variability. The Taurus Mountain Range is divided into sub-regions, using the WWF HydroSHEDS Basins Level 3 dataset and the Köppen–Geiger climate classification map, and in 100-m elevation bands. The temporal variability of snow cover is quantified by the Regional Snowline Elevation (RSLE). The Regional Snowline Elevation (RSLE) is estimated in Google Earth Engine (GEE) using the methodology developed by Krajci et al. (2014). The temporal trends of the annual number of snow cover days (Dsc), for the different elevation zones in each sub-region, are derived from the RSLE time series and are analyzed using a modified Mann-Kendall (MK) non-parametric test. The sensitivities of Dsc to the inter-annual variability of winter temperature and precipitation and the snow cover duration trends are estimated in each tile and for all elevation bands in all sub-regions. In general, the analysis carried out, considering its limitations and uncertainties, found that there is no reason to be concerned about future water shortages in the area of the Taurus Mountain Range due to the decrease in the amount of water stored as snow. This is a positive outcome that indicates that there are no significant future changes in snow cover patterns and, as a result, the availability of water in the region will not be at risk.

Contents

List of Figures

List of Tables

List of abbreviations

D_{SC} annual number of snow cover days

DEM Digital Elevation Model

ERA5 ERA5-Land Daily reanalysis dataset

GEE Google Earth Engine

GMTED2010 Global Multi-resolution Terrain Elevation Data 2010

MOD10A1 V6 MODIS/Terra Snow Cover Daily L3 Global 500m SIN Grid - Version 6

NDSI Normalized Difference Snow Index

ROI Region Of Interest

RSLE Regional Snowline Elevation

SWE Snow Water Equivalent

TMR Taurus Mountain Range

1 Introduction

1.1. Problem statement

Worldwide, more than one billion people rely on seasonal snow to meet their water needs [1, 2]. Agricultural, industrial, and drinking water supplies are largely dependent on the melting of seasonal snow, especially in the Northern Hemisphere [3, 4].

In the areas where snowmelt dynamics dominate the hydrological cycle, numerous factors indicate its importance on human life, plant and animal ecosystems, and the earth's climate. First, snow accumulation and melting regulate the magnitude and timing of high and low flows [2, 5]. Changes in the amount of water stored as snow and/or in the snow melt period are going to severely affect human activities and the environment in the downstream water basins. In addition, the melting of seasonal snow regulates the duration of the growing season. Alterations in the duration of the growing season affect agricultural productivity and forest growth, positively or negatively. In addition to ecosystems, these changes in vegetation cover and carbon storage can affect climate systems [6]). Finally, the climate of the Earth is also influenced by changes in seasonal snow cover that regulate land surface temperature through albedo feedback [7].

Several factors control snow cover and snowmelt dynamics. The main climatic drivers are temperature and precipitation [8, 9]. Furthermore, snow accumulation and melt depend on solar radiation [10], vegetation dynamics [9], topography [11], and wind, which regularly produces snowdrifts [12]. Snowmelt and snow accumulation are processes that vary largely spatially and temporally, especially on a small scale, due to variations in the surface energy balance and in sensible heat advection, see Refs [13, 14, 15].

The purpose of this study is to quantify the local and regional dynamics of snow cover in Taurus Mountain Range (TMR) in Turkey and to identify the main climatic drivers responsible for the variability of the detected snow cover. More specifically, this study aims to identify whether it is reasonable to assume that water shortages, as a result of the decrease in snow cover, will occur in the Taurus Mountains and surrounding area in the future. Investigating spatial patterns of snow cover dynamics is performed in the different regions of the Taurus Mountain Range to identify areas prone to changes in seasonal snow.

1.2. Research objectives

Compared to various remote sensing snow cover studies focusing on small / catchment scales [16, 17], with limited spatial context, or continental scales [18, 19, 20], which cannot provide detailed information on a specific region, this study investigates local and regional spatial patterns and temporal dynamics of snow cover in a specific mountain range of interest.

Large-scale systematic snow cover analysis is performed using a data-based approach based on satellite observations throughout the Taurus Mountain Range (TMR). The advantage of data-based studies over widely used modeling studies is their robustness against additional—inherent in the modeling process—uncertainties, e.g., Refs [21, 22].

In general, the objectives of this study are the following:

1. Quantification of temporal variability in snow cover in different sub-regions of the TMR.
2. Identification of regional differences and analysis of the trends.
3. Investigating the sensitivity of annual snow cover duration to inter-annual climatic variability.

1.3. Research questions

The questions that must be answered to achieve the objectives described in Section 1.2 are the following:

1. What is the temporal variability of Regional Snowline Elevation (RSLE) across TMR?

   Temporal variations in RSLE indicate changes in snow cover and snowmelt duration [16]. Calculating the RSLE is also used to improve the accuracy and availability of cloud-affected snow cover products [17, 23].

2. Are there significant increasing or decreasing trends in monthly and annual number of snow cover days (D_{SC}) throughout the Taurus Mountain Range?

   The D_{SC} is derived from the RSLE time series. The spatial patterns of systematic changes in D_{SC} were examined from 2000 to 2019 in the Taurus mountain range.

3. What is the effect of certain climatic variables, such as winter temperature and precipitation, on D_{SC}?

   Analyzing the spatial variability of sensitivities of climatic variables indicates in which sub-region and elevation zone the snow cover duration is going to be influenced more by changes in the climatic variables, i.e., winter temperature and precipitation.

1.4. Thesis outline

In the following section, the outline of the thesis is presented. Chapter 2 consists of a short review of previous studies and information on Google Earth Engine (GEE), a cloud service used to process large geospatial data. In Chapter 3, the study area and the reasons for its selection are presented. The datasets and methods used in the present study are presented in Chapter 4. The results and the discussion of the results are presented in Chapter 5 and the main conclusions and reccomendations are presented in Chapter 7.

2

Background theory

2.1. Snow metrics

Several metrics are used to quantify snow patterns and dynamics. The most important snow metrics are the following:

- Snow Water Equivalent (SWE),
- Snow Depth,
- Snow Covered Area,
- Snow Cover Duration.

The choice of the most appropriate snow metric depends on the scale of the application. Snow metrics with higher information content, such as SWE, cannot be used in global– or regional–scale problems, while lower-dimensionality metrics, such as the snow-covered area, can provide more reasonable representations of spatial and temporal patterns of larger areas.

Despite the fact that SWE is the most informative snow metric for hydrological and water resource applications, the inability to reliably quantify it, with the existing available technology, at global and regional spatial scales, has led researchers to widely use other readily observable snow metrics, i.e., snow depth (e.g., Refs [24, 25, 26]), snow covered area (e.g., Refs [27, 28, 29]), snow cover duration (e.g., Refs [30, 19, 31]).

2.2. Remote sensing snow cover products

A growing number of published studies on snow-related topics use remote sensing products. Recent technological developments have highlighted the importance of remote sensing products in snow cover mapping for regional and global-scale applications due to their ability to provide detailed spatial and temporal information. Remote sensing products, despite possible limitations due to cloud cover [32], are especially useful for regions without ground measurement stations [33].

The main issue when choosing the appropriate remote sensing product is the trade-off between temporal and spatial resolution. Several remote sensing products have previously been used for snow cover studies. For large-scale applications, the weekly 4 km NOAA-AVHRR snow cover product [34, 19, 29, 35] and the 30 m Sentinel 2 or LANDSAT products [36, 37, 38] are frequently used. Remote sensing products with low temporal resolution have higher spatial resolution, and vice versa. Therefore, a balance must be achieved between the ability to identify spatially complex patterns and the maintenance of a relatively high temporal resolution. As explained in Chapter 4, the MODIS Terra Snow Cover Daily Global 500m data set is used, as it provides a good compromise between spatial and temporal resolution.

In general, it is relatively common to investigate seasonal snow using models [39, 40, 41]. This approach is prone not only to errors in the data but also to errors in the modeling process itself [21]. To date, remote sensing studies have investigated the variability of snow cover on global scales [19, 31]

or catchment scales [16]. At global scales, local and regional snow cover patterns cannot be identified, while, at catchment scales, the spatial context is limited, despite the higher spatial resolution.

2.3. Google Earth Engine (GEE)

GEE is a cloud-based service for processing large geospatial data, for both commercial and non-commercial users.

It is a powerful platform that contains freely available geospatial datasets that can be found in many different sources, and powerful tools that can be used to easily perform analyses and calculations with large amounts of data [42].

The organized inventory of remote sensing datasets provided in the platform, and the cloud-based nature of GEE, facilitate efficient data acquisition and processing. The data catalog provided contains several datasets useful for environmental studies, for example, temperature, precipitation, elevation data, etc.

The cloud-based nature of GEE does not require the downloading of decades of daily images on the local computer. For example, downloading all daily snow cover, temperature and precipitation images for the present analysis would require more than 1 terabyte of local memory and many days to download all the data.

GEE uses concurrently multiple servers to perform calculations. This approach of parallel computations significantly reduces the computational time. To utilize this advantage of GEE, the code must be constructed in a way appropriate for parallel computations. This requires functions to be created and mapped onto the data structures. Loops and if statements must not be used because they increase computational cost.

The data structures used most often are features and images. Images are typical raster datasets that can have multiple bands, and features are geometries that contain additional information, i.e., properties. Multiple images can be packed together to create an image collection. For example, a year of daily Sentinel-1 images creates an image collection with 365 images. Similarly, when multiple features are packed together, they create a feature collection. The GEE user can construct a new function or can use one that already exists in the GEE library.

The RSLE method used in the present analysis to calculate the duration of snow cover in TMR is implemented in GEE. Calculating the RSLE in GEE is extremely efficient, but requesting data from the server to the client side can often be tricky. Earth Engine uses Google clusters to do the computations in parallel. If some clusters do not work when the data are requested, the execution of the code stucks and additions techniques must be implemented, e.g., asynchronous programming, timeout functions, etc.

3

Study area

The following chapter describes the study area, i.e., the Taurus Mountains, and analyzes the reasons for its selection.

3.1. Area description

The Taurus Mountains, presented in Figure 3.1, part of the Alpine-Himalayan orogenic belt, are a mountain range in southern Turkey. They extend along the Mediterranean coast of Turkey from Lake Eğirdir to the upper part of the Euphrates [43].

The mountain range is divided into three chains:

1. Western Taurus (Turkish: Bati Toroslar),
2. Central Taurus (Turkish: Orta Toroslar) and
3. Southeastern Taurus (Turkish: Guneydogu Toroslar).

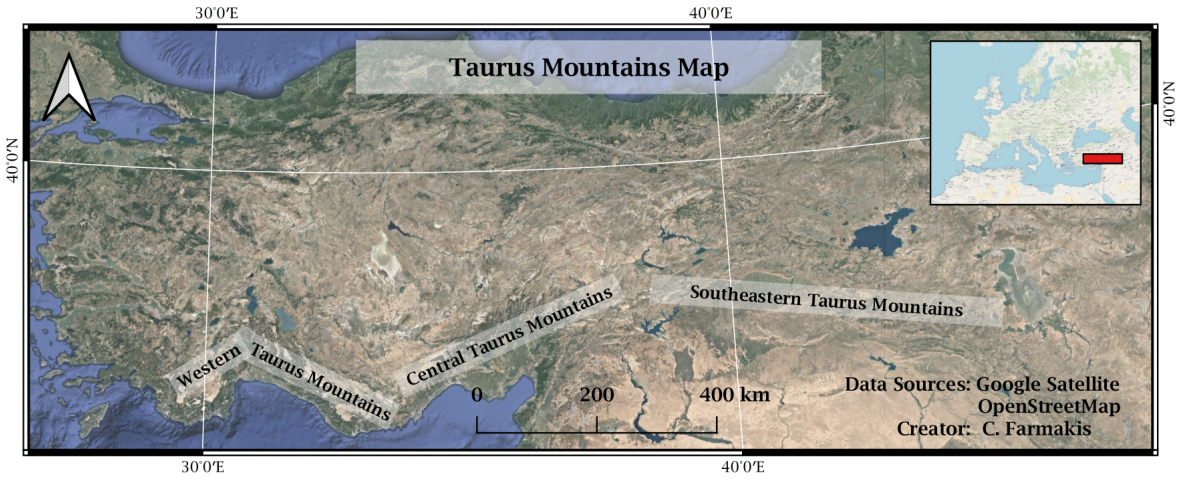

Figure 3.1: Location of the Taurus mountains

The current name of the mountain range was first mentioned by Polybius, a Greek historian who lived from 202 BC to 120 BC, as Ταῦρος (English: Taurus), which means bull, in his book "Histories" (Ancient Greek: Ἱστορίαι) [44]. The most likely exegesis is that the Taurus Mountains were named after the bull, which represented the ancient Near Eastern storm gods. A plethora of ancient storm god temples can be found in the Taurus Mountains [45, 44].

Figure 3.2 illustrates the elevation map of the wider Taurus Mountains area. Mount Kizlarsivrisi (3.086 m) is the highest peak of the western Taurus Mountains and Mount Demirkazık (3.756 m) is

the highest peak of the central Taurus Mountains. The southeastern Taurus Mountains are part of the Tigris and Euphrates basins and a border of Mesopotamia with Anatolia [44].

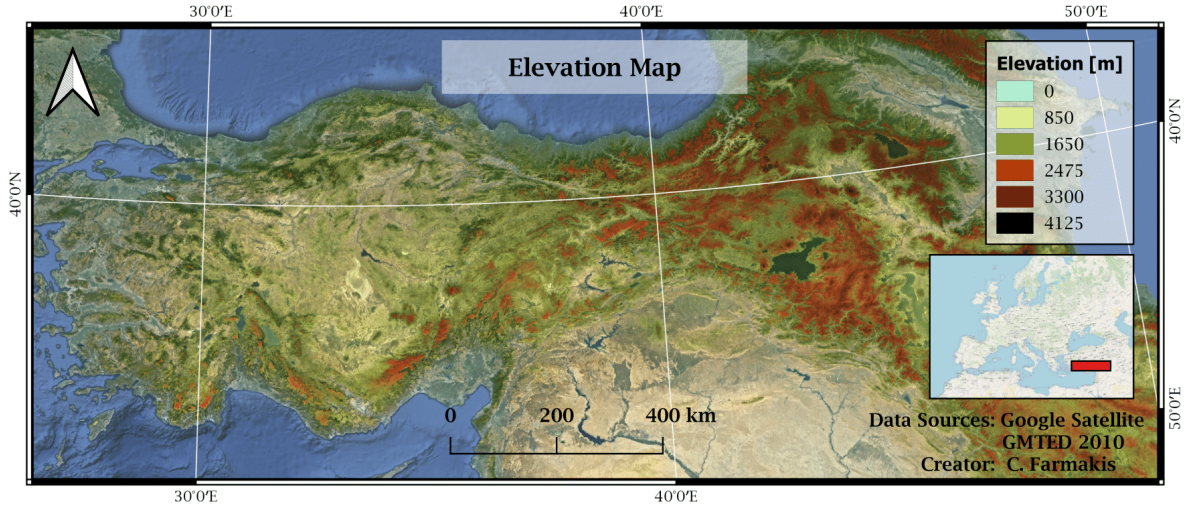

Figure 3.2: Elevation map of the Taurus mountains

Figure 3.3 illustrates the land use map of Turkey, where it can be seen that the dominant land use in the TMR is forests and semi-natural areas. Evergreen oak forests, Turkish pine and macchia shrubs are found at elevations below 1200 m [44]. At higher elevations, Cilician fir, Lebanon cedar, juniper, and black-pine forests are common [44].

The climate of the area is analyzed in Section 4.2. In general, the climate is Mediterranean in the south, with hot dry summers and rainy winters, cold semi-arid in the north, and humid continental at higher elevation, with precipitation throughout the year.

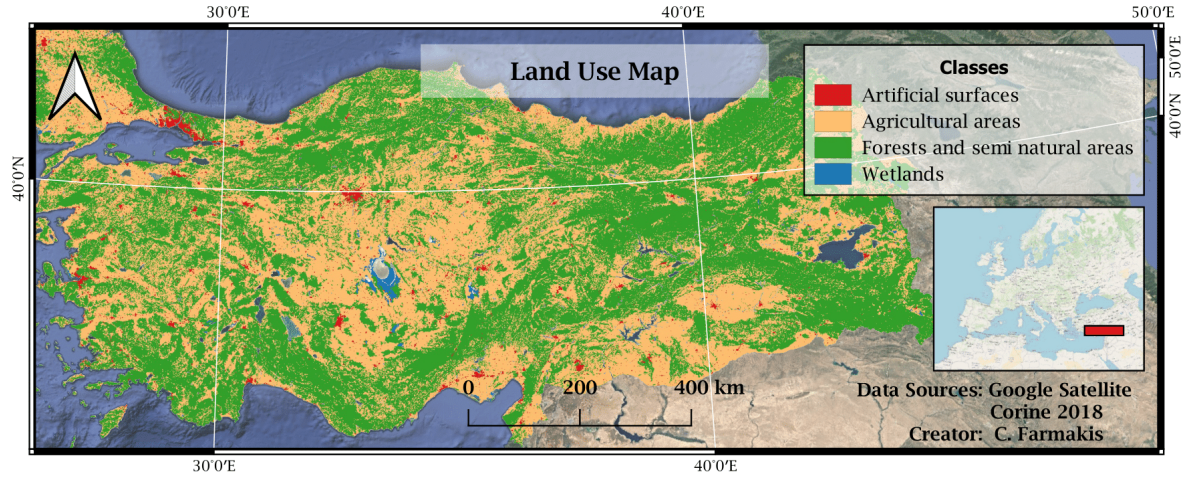

Figure 3.3: Land use map of the Turkey

3.2. Area importance

Investigation of snow cover in the TMR is important because meeting human water demand in the region from March to August is highly dependent on snowmelt [4].

Spring and summer runoff from snowmelt is an important water resource for 305 of the 421 basins studied in the northern hemisphere; however, rainfall runoff adequately covers spring and summer human water demand in 280 of the 421 basins [4]. The basins that depend on snowmelt runoff and are prone to have unmet demand by 2060, due to decrease in summer and spring precipitation, are mainly located in the subtropical zone of the northern hemisphere. These basins are called snow-sensitive

and are found to be 97 [4]. Figure 3.4 shows that there are snow-sensitive basins (with purple and maroon colors) in the TMR.

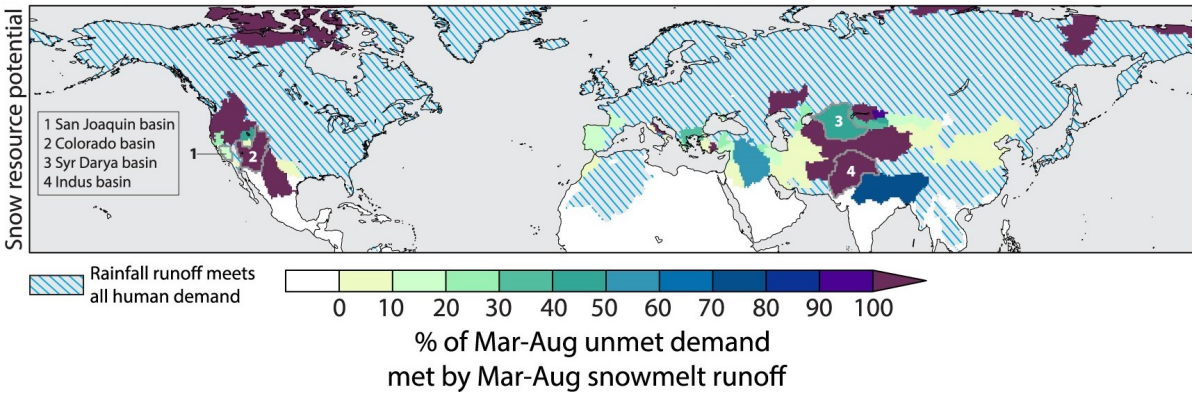

Figure 3.4: The snow resource potential. Adapted from “The potential for snow to supply human water demand in the present and future” [4], Environ. Res. Lett., 1–10, Creative Commons Attribution 3.0 license.

4

Data & Methods

4.1. Data

The different datasets used are explained and discussed in the following section.

4.1.1. MODIS Terra Snow Cover Daily Global 500m

There are several remote sensing products that provide snow cover information. Choosing the appropriate product is challenging and requires evaluating the trade-off between the spatial and temporal resolution of the remote sensing products. Products with higher spatial resolution have lower temporal resolution and vice versa. Snow cover products with lower spatial resolution are not appropriate for identifying spatially complex snow patterns, e.g., in mountain ranges, whereas products with low temporal resolution might fail to resolve the temporal snow cover dynamics. In this study, the MODIS/Terra Snow Cover Daily L3 Global 500m SIN Grid - Version 6 (MOD10A1 V6) product was used because it provides a suitable compromise for regional snow cover studies, e.g., Refs [46, 47, 48]. The spatial resolution is equal to 500 m, and the temporal resolution is daily.

MOD10A1 V6 data are obtained by the Moderate Resolution Imaging Spectroradiometer (MODIS) carried by the Terra Satellite (EOS AM-1). Terra is a NASA satellite whose mission is to measure Earth's atmosphere, hydrosphere, and lithosphere for research purposes, such as studying the climate system [49].

MOD10A1 V6 product comprises daily gridded snow cover, fractional snow cover, snow albedo, and quality assessment information. The Normalized Difference Snow Index (NDSI) is utilized to determine snow cover, and several filters are applied to flag inaccurate and erroneous snow cover finding, for example due to cloud obstruction.

The MOD10A1 V6 product used is openly available on the GEE platform.

4.1.2. Global Multi-resolution Terrain Elevation Data 2010 (GMTED2010)

Calculating the RSLE time series requires Digital Elevation Model (DEM) of the area. For this purpose, the USGS EROS Archive - Digital Elevation - Global Multi-resolution Terrain Elevation Data 2010 (GMTED2010) [50], with a resolution of 7.5 arc seconds, is used. The version of GMTED2010 used is called the "Breakline Emphasis" and its main characteristic is that it preserves key features of the landscape, such as rivers and mountain ridges.

GMTED2010 is mainly a product of NGA's one-arc-second, void-filled SRTM Digital Terrain Elevation Data (DTED) [51], which was developed to replace the GTOPO30 Elevation Model. Gaps and out-of-coverage areas in the SRTM data were filled using several other DEMs, such as the Canadian Digital Elevation Data (CDED), the National Elevation Dataset (NED) for the United States of America, an Antarctica satellite radar and laser altimeter DEM, etc. [50]. GMTED2010 outperforms GTOPO30 in terms of consistency and accuracy [50], but there are still many areas where the accuracy of [50] is poor due to the scarcity of reliable elevation data.

GMTED2010 is an appropriate DEM for regional, continental, and global analyses. GMTED2010 is ideal for identifying the spatial-temporal patterns of snow cover in TMR, due to its resolution, which is detailed enough for the extent of the study area, and due to the lack of freely available local DEMs.

4.1.3. ERA5-Land Daily reanalysis dataset

The climatic drivers of snow cover examined were derived from temperature and precipitation data extracted from ERA5 Daily Aggregates - Latest Climate Reanalysis Produced by the ECMWF / Copernicus Climate Change Service [52, 53].

ERA5-Land Daily reanalysis dataset (ERA5) dataset is a product of global observations and model data. An advantage of the daily ERA5 dataset is that it provides consistent daily global data from 1979 for the following parameters:

- air temperature at 2 m,
- maximum air temperature at 2 m (calculated on the basis of hourly values of air temperature at 2 m),
- minimum air temperature at 2 m (calculated on the basis of hourly values of air temperature at 2 m),
- dewpoint temperature at 2 m,
- total precipitation,
- mean sea-level pressure,
- surface pressure,
- South to North (v) and West to East (u) components of the wind at 10 m

The total daily precipitation is the sum of the measured hourly precipitation, while all other parameters are the daily means of the hourly data[52].

ERA5 dataset is openly available in the Copernicus Climate Data Store and can also be accessed on the GEE platform.

4.1.4. WWF HydroSHEDS Basins Level 3

The WWF HydroSHEDS Basins Level 3 dataset is used to provide the watershed boundaries in TMR.

HydroSHEDS provides information on several scales, suitable for regional and global scale applications. In addition to the watershed boundaries, the HydroSHEDS data set includes the following [54, 55]:

- river networks,
- flow accumulations, and
- drainage directions.

The watershed polygons have been created using NASA's SRTM elevation data, with a resolution of 15 arc-seconds. The quality of the data set decreases in places without SRTM elevation data, for example, above 60 degrees latitude, where a coarser DEM is used [54, 55]. For the present investigation, the appropriate scale for the watersheds was level 3.

WWF HydroSHEDS is an open access data set, developed by the WWF Conservation Science Program, and can be accessed on the GEE platform.

4.1.5. Köppen–Geiger climate classification system

The Köppen–Geiger climate classification system is used to divide TMR into different regions according to the climate of each region.

This classification system introduces five different climate groups that are further divided into more groups according to the temperature and precipitation patterns [56, 57].

This widely used climate classification was introduced by Wladimir Köppen [56] and was modified several times by Köppen and other climate scientists [58, 57]. The most notable adjustments have been made by Rudolf Geiger [59, 60].

4.2. Methods

In the following chapter, the process of calculating the spatiotemporal patterns and trends in the duration of snow cover, and the sensitivity of the annual number of snow cover days to the interannual climatic variability is presented.

4.2.1. Regional Snowline Elevation (RSLE) method

To calculate the elevation of the snow line elevation (RSLE), preserving the daily temporal resolution of the cloud-affected MODIS snow cover data set, the methodology developed by Krajci et al. (2014) [16] is used.

The main idea is to divide the region into 'tiles', i.e. specified spatial domains, loop from lowest to highest elevation of each 'tile', and calculate, for each time step, the elevation where the sum of snow-covered pixels below and land pixels above is minimized.

Figure 4.1 shows the map of the examined Region Of Interest (ROI), which includes the Taurus Mountains.

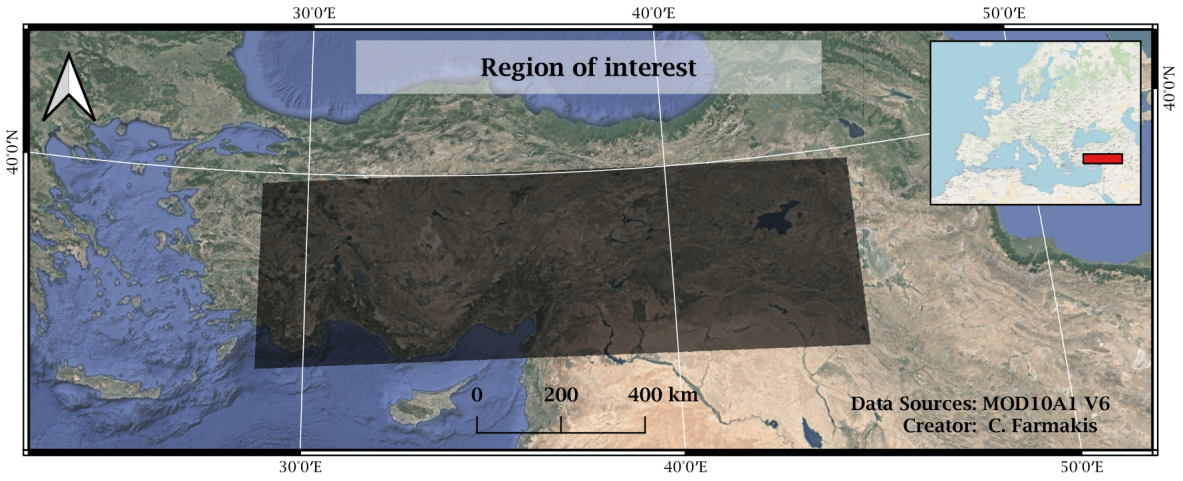

Figure 4.1: Region of interest

To loop from the lowest to the highest elevation of each tile, a specific elevation step must be chosen. In the present analysis, a different approach is chosen, proposed by van Esch (2019) [61] to reduce the computation time. According to this approach, the elevation bands are not created using a constant elevation step, but by calculating the elevation percentiles of every 'tile' from the 2nd to the 98th percentile with a step of two.

A pixel is initially considered snow covered if the normalized difference snow index (NDSI) is greater than a selected specific threshold value, e.g., NDSI is equal to 0.4. Having calculated the daily RSLE of the 'tiles', a pixel is ultimately defined as snow covered on a specific day if the elevation of the pixel is higher than the RSLE of the tile to which it belongs.

The script for implementing the RSLE methodology was originally developed by van Esch (2019) [61] and is modified by the author of the present analysis (see Appendix C).

4.2.2. Choice of 'tile' size

Applying the RSLE methodology requires dividing the spatial domain examined into smaller domains, called 'tiles'. In each 'tile', a snow line elevation value, representative of all pixels in the 'tile', is calculated.

Larger 'tiles' filter out the natural variability of the RSLE within the 'tile', resulting in smoother time series. When choosing a smaller 'tile' size, cloud cover affects the generation of continuous RSLE time series, resulting in the appearance of more gaps.

Moreover, the 'tile' size determines the computation time. Choosing a smaller 'tile' size is computationally more expensive and does not necessarily increase the information gained. When smaller 'tiles' are chosen, the fraction of missing pixels in each 'tile' is going to increase since fewer pixels exist in each 'tile' and cloud cover will result in more 'tiles' being discarded. The threshold in the fraction of

missing pixels, above which the RSLE values calculated for a specific day in a ‘tile’ are discarded, is analyzed in Section 4.2.4.

In the present analysis, two different ‘tile’ sizes, 30 and 50 km, were examined. Figures 4.2 and 4.3 illustrate these two sizes of ’tiles.’

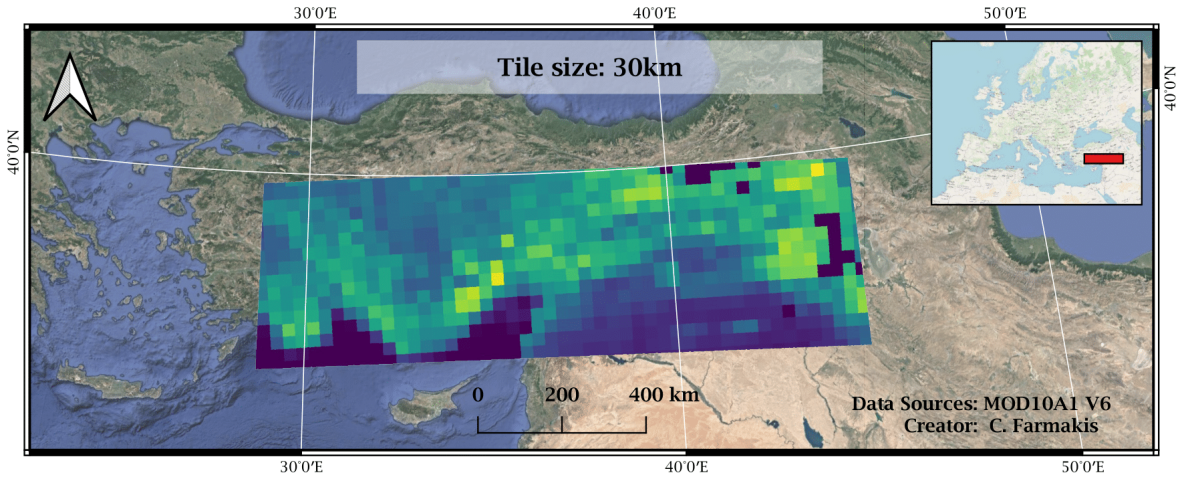

Figure 4.2: ‘Tile’ size equal to 30 km.

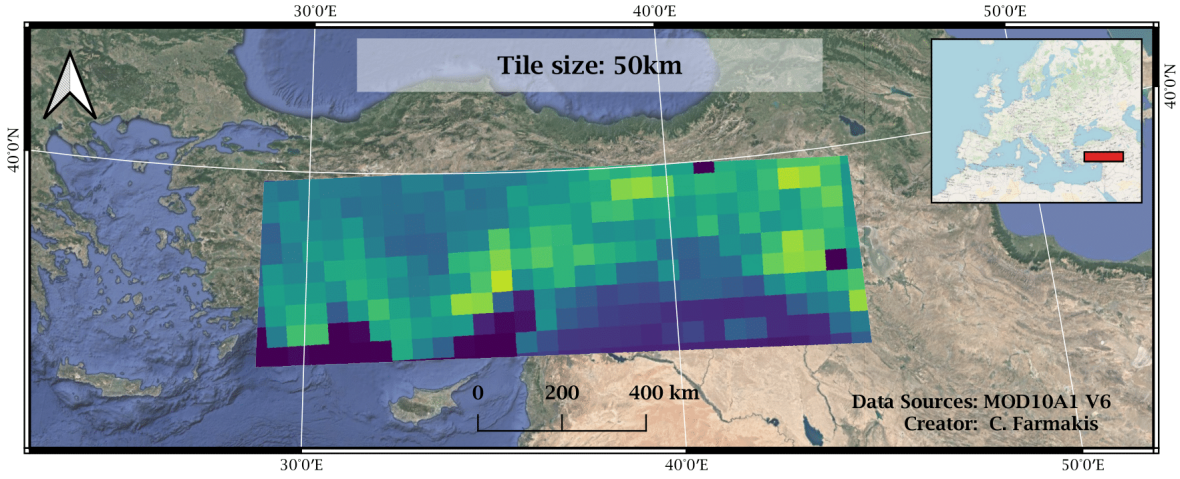

Figure 4.3: ‘Tile’ size equal to 50 km.

4.2.3. Choice of missing pixel threshold

When calculating the RSLE values, the percentage of missing pixels is also calculated for each ‘tile’ and for each day. The snowline elevation values calculated with very few pixels need to be discarded as unreliable. The maximum percentage of missing pixels in a ‘tile’, above which the number of pixels is not sufficient to calculate the snowline elevation, is not known. In the present analysis, two missing-pixel thresholds have been applied, 0.5 and 0.7. If the fraction of pixels missing in a tile, e.g., due to cloud cover, is higher than the specified threshold, the RSLE value is discarded in this specific tile for this specific day.

Figures 4.4 to 4.6 illustrate the number of gaps greater than 8 days in the daily RSLE time series for different missing pixel thresholds applied.

The lower the missing-pixel threshold applied, the more gaps in the RSLE time series. Applying a missing-pixel threshold results in smoother RSLE time series for both ‘tile’ sizes, because noisy RSLE values derived from tiles with very few pixels are removed. For the present analysis, a missing

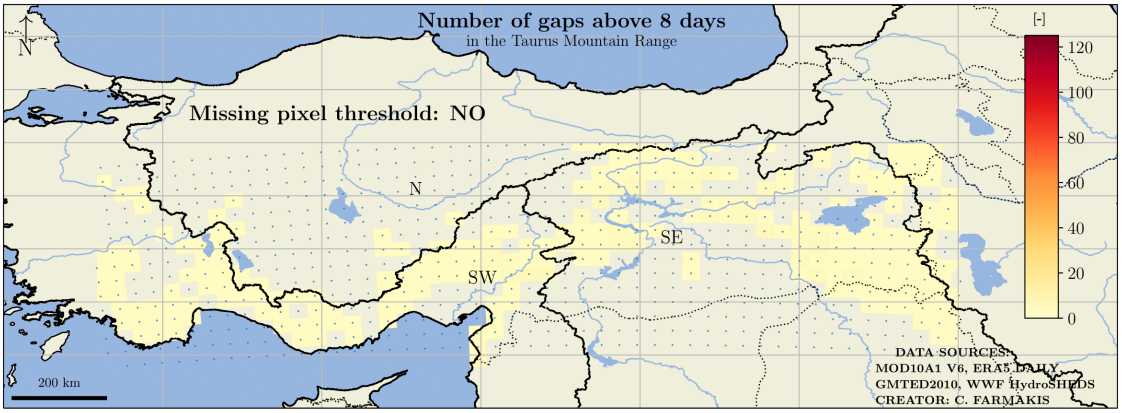

Figure 4.4: Number of gaps greater than 8 days in the daily RSLE time series when the missing pixel threshold is not applied.

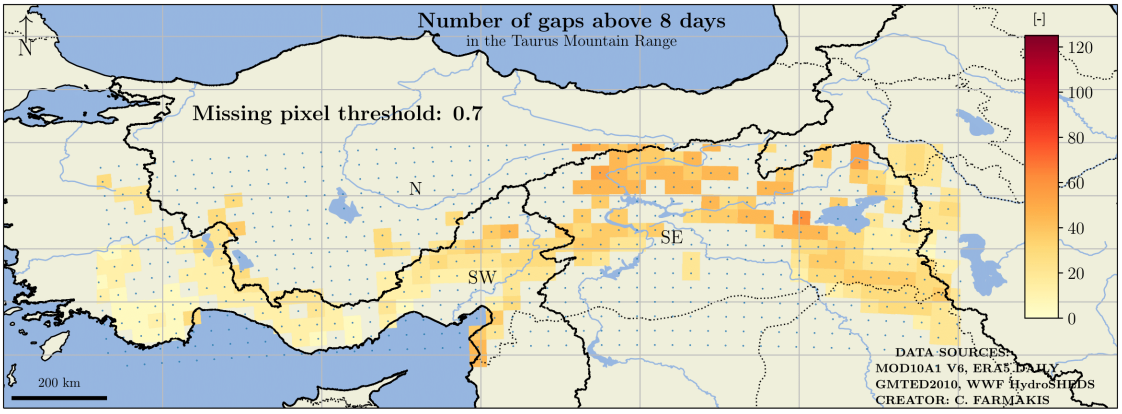

Figure 4.5: Number of gaps greater than 8 days in the daily RSLE time series for missing pixel threshold equal to 0.7

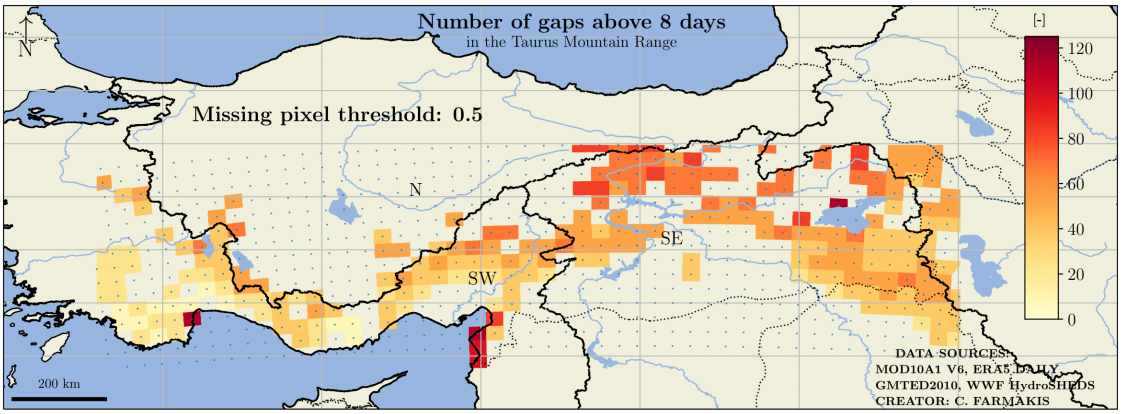

Figure 4.6: Number of gaps greater than 8 days in the daily RSLE time series for missing pixel threshold equal to 0.5

pixel threshold equal to 0.7 is chosen as a trade-off between creating more gaps, which means losing information, and acquiring noisier RSLE time series.

4.2.4. RSLE post-processing

After calculating the RSLE time series for all tiles for the 20-year period, certain processing steps must be performed before calculating the annual number of snow cover days.

Post-processing of the RSLE time series requires the following steps:

1. 'Tiles' with a mean elevation below zero are discarded.

   This applies to 'tiles that are located in the see or other water bodies.

2. ‘Tiles’ where the difference between maximum and minimum elevation is greater than 300 m are discarded.

   The reason for this is to avoid areas constantly covered in snow in lower elevations.

3. The RSLE difference between two consecutive days may not be greater than 80% of the local elevation range.

   The RSLE values on a specific day for a specific ‘tile’ found to be greater are discarded.

4. Discard the ‘tiles’ that have an RSLE time series that seems not to vary.

   After visually inspecting the RSLE time series of all ‘tiles’, the ‘tiles’ where the difference between the minimum and the maximum snowline elevation value is lower than an arbitrary threshold. The snowline cannot be constant or approximately constant, because this would mean that the tile is snow covered the entire time, and this is not possible since there is no permanent snow in the region.

5. Apply a linear interpolation to fill the gaps in the RSLE time series.

   More sophisticated interpolation methods are not useful because the uncertainties in the data are large and a more sophisticated method would be computationally more expensive without providing any additional value.

These post-processing steps have been applied to both ‘tile’ sizes and to all missing pixel thresholds examined.

4.2.5. Divide the TMR into sub-regions

To answer the first research question, which is to identify the spatiotemporal variability of the RSLE, the first step is to divide the region of interest, that is, the Taurus Mountain Range (TMR), into subregions based on topography and dominant climatic characteristics.

First, the WWF HydroSHEDS Basins Level 3 data set (see Section 4.1.4) is used to divide the region. The outlines of the three basins in the region are presented in Figure 4.7a.

Figure 4.7b illustrates the Köppen–Geiger climate classification map of the Taurus Mountains, where it can be seen that the three basins presented above correspond approximately to three different climate classes. The northern basin in central Turkey is characterized by a cold semi-arid climate (BSk), the southwestern basin along the Mediterranean coast is characterized by a hot summer Mediterranean climate (Csa), and the eastern basin is characterized by a humid continental climate (Dsa).

Figure 4.7 illustrates (a) the WWF HydroSHEDS Basins Level 3 map [62] and (b) the Köppen–Geiger climate classification map of the Taurus mountains.

4.2.6. Calculate the monthly and annual number of snow cover days (D_{SC})

The annual—and monthly—number of snow cover days (D_{SC}) is computed from the RSLE time series, after the processing explained in Section 4.2.4, both for each tile and for each sub-region described in Section 4.2.5.

The whole ROI and the described sub-regions have been stratified into 100-m elevation bands. The ‘hydrological year’, which starts at October 1, has been used for the estimation of the D_{SC}, to capture the snow accumulation and melt cycles.

If daily RSLE value of a tile is higher than the elevation of a pixel in this ‘tile’, the pixel is described as snow covered for this specific day. The sum of the snow-covered days in a ‘hydrological year’ results in the D_{SC} for this pixel. A ‘tile’ is defined as snow covered for a specific day if more than half of the pixels are defined as snow covered. The ‘tiles’ found to be snow covered throughout the entire year and the ‘tiles’ that do not have at least one snow covered day during a whole year are discarded from the analysis.

The annual and monthly number of snow covered days for TMR and its subregions and elevation bands were calculated using a bootstrapping approach, and the probability distribution functions for each year have been calculated and presented as box plots in Section 5. The median, mean, 25th, and 75th percentiles have been identified and the annual trends in these values have been examined, as explained in Section 4.2.7.

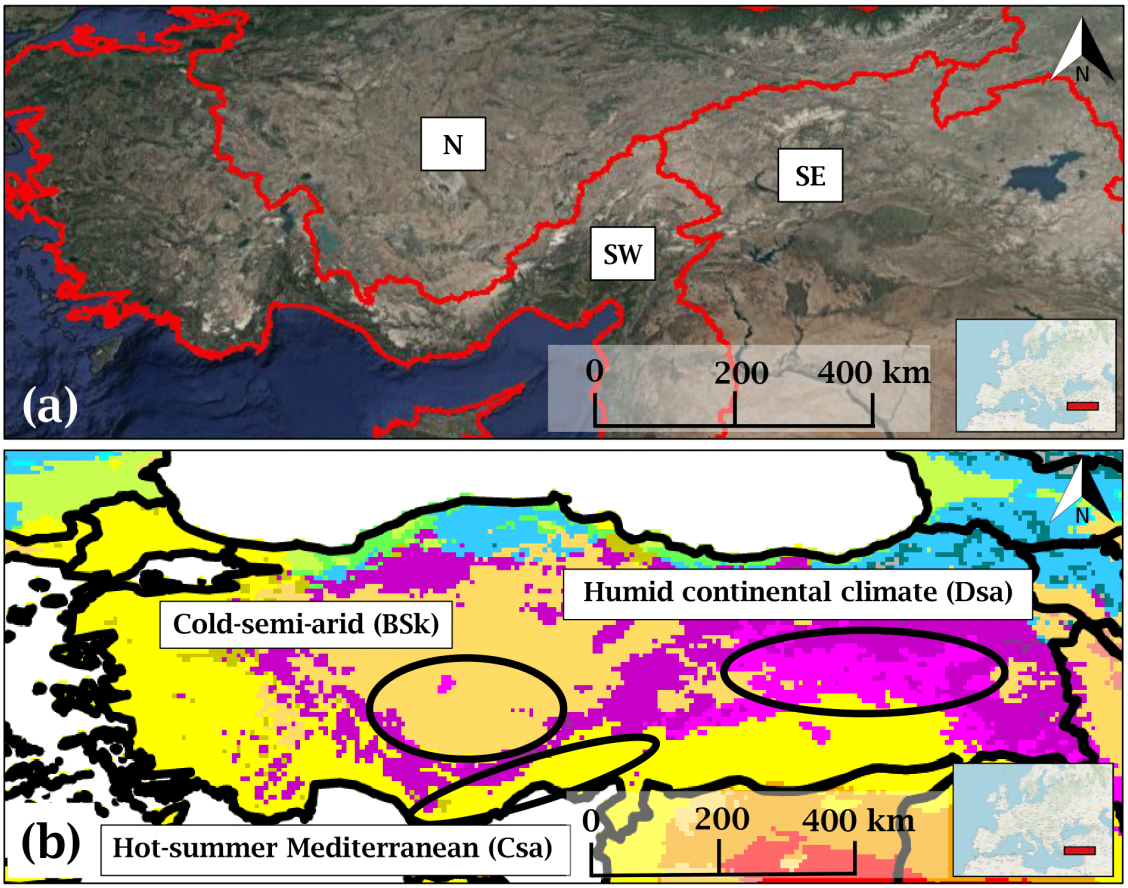

Figure 4.7: (a) WWF HydroSHEDS Basins Level 3 map [62]; (b) Köppen–Geiger climate classification map of the Taurus mountains [63, 64]

4.2.7. Calculating the temporal trends

The rate of change in the annual and monthly number of snow covered days and in the monthly average RSLE values was estimated using the Theil-Sein estimator [65, 66], which requires fitting linear trends into the annual data.

Spatial patterns and systematic changes of the variables of interest were examined throughout the TMR, from 2000 to 2019, using the modified Mann-Kendall (MK) non-parametric test [67]. The advantage of this modified MK test is that it addresses serial autocorrelation issues. Trend slopes and p-values are presented in Section 5.

There were no in situ snow cover measurements to perform additional analysis and comparisons with the MODIS-derived snow cover data.

4.2.8. Sensitivity of D_{SC} to inter-annual climatic variability

The sensitivity of the annual number of snow covered days D_{SC} to inter-annual climatic variability was examined for all sub-regions, elevation bands and 'tiles' in the TMR.

Assuming that precipitation and temperature are the two most important factors that affect snow cover, two different pairs of climatic drivers were examined as the main controls of the D_{SC}.

The first pair of climatic drivers examined is the following:

1. Mean temperature for 6 months (November - April)
2. Total precipitation for 6 months (November - April)

The second pair of climatic drivers examined are the following:

1. The annual number of days with a mean temperature below zero.

2. The annual sum of precipitation on days when the temperature was below zero, which is a proxy for solid precipitation.

The results of the second pair of climatic drivers are presented in Appendix B.

Analyzing the spatial variability of the sensitivities of D_{SC} is carried out in order to find in which sub-region and elevation zone snow cover duration will be more influenced by changes in the climatic variables of interest.

The sensitivity of D_{SC} to the inter-annual variability of temperature and precipitation is examined by assuming individual linear relationships of D_{SC} with the climatic driers, together with a linear combination of the two climatic variables as independent variables. The adjusted R2 metric is used to account for the different predictors [66].

Sensitivities are estimated in each tile, for all elevation bands in all sub-regions. The calculated sensitivities must be corrected to account for the correlation between the two climatic variables, which had initially been mistakenly individually related to D_{SC}. Sensitivities were calculated and corrected using the equations presented by Liu (2020) in Chapter 3.3.1 [68].

By examining the sensitivities in the different sub-regions and elevation bands, the spatial patterns of the impacts that potential changes on the climatic drivers might have on D_{SC} are analyzed.

5

Results & Discussion

In the following chapter, the results of the analysis and the discussion of the results are presented.

5.1. Monthly number of Snow Cover Days (SCD) for all elevation bands

Figure 5.1 shows the monthly number of snow covered days for all months and elevation bands from 2000 to 2019.

Each month is presented in a different sub-figure. Each sub-figure illustrates the inter-annual variability of the number of snow-covered days in this month, for all elevation bands.

The trends of all lines have been calculated (see Section 4.2.7) and the p-values found are presented in Figure 5.2 to assess if there are significant upward or downward trends in the number of snow cover days for the different months and elevation bands.

Figure 5.2 illustrates the table with the calculated p-values for all months and elevation bands. The lower the p-value, the more significant the upward or downward trend. Lower p-values are presented in a darker blue color, and higher p-values are presented in lighter shades, with p-values equal to one being presented with a white color.

Figure 5.3 illustrates the change, in days per decade, in the monthly number of snow covered days for all months and elevation bands. Negative trends, which occur when the monthly snow covered days are reducing, are colored red, and positive trends, which occur when the monthly snow covered days are increasing, are colored blue. The more pronounced the change, the darker the shades of blue and red, for increasing and decreasing trends, respectively.

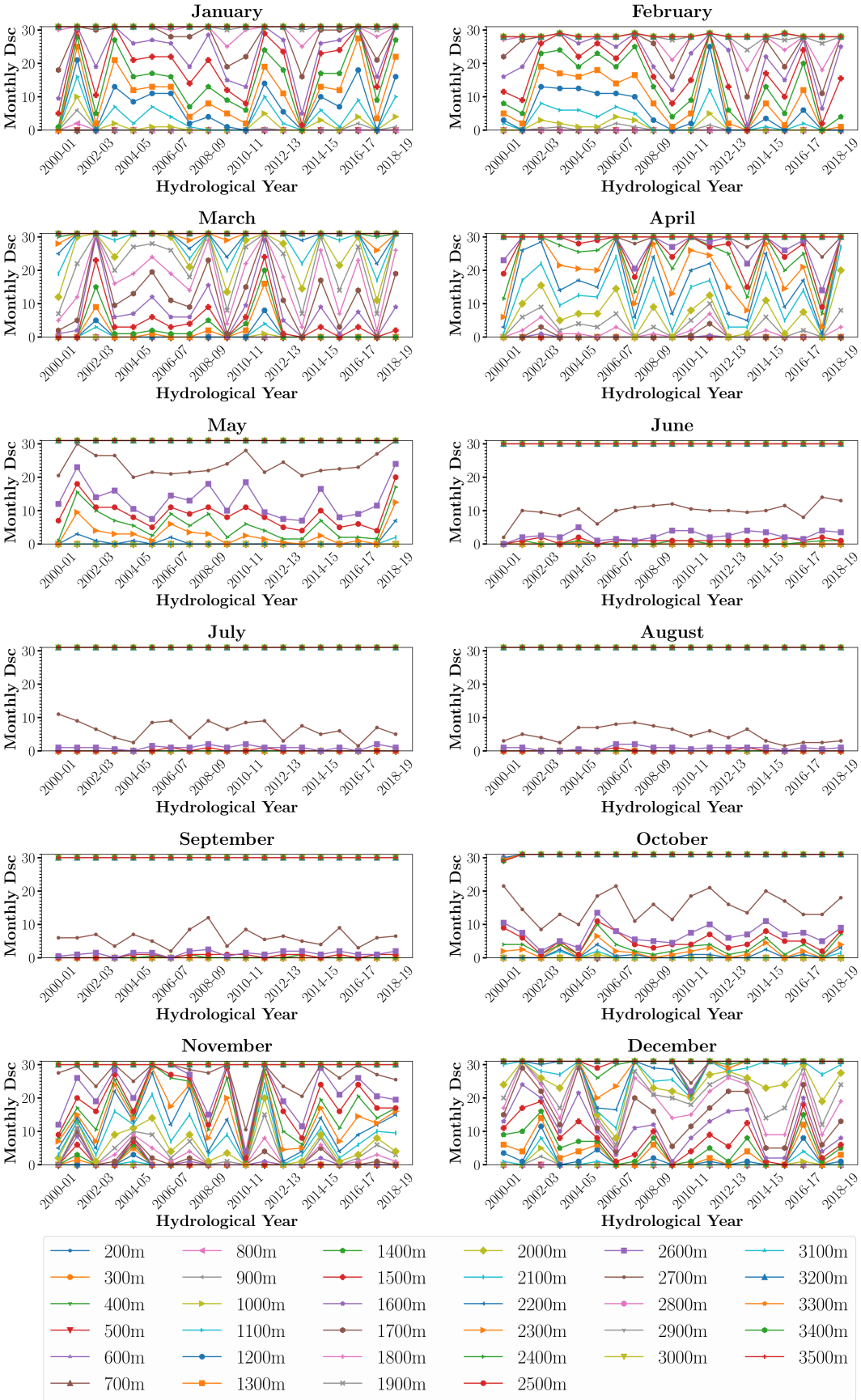

Figure 5.1: Snow covered days in all elevation bands for all months from 2000 to 2019

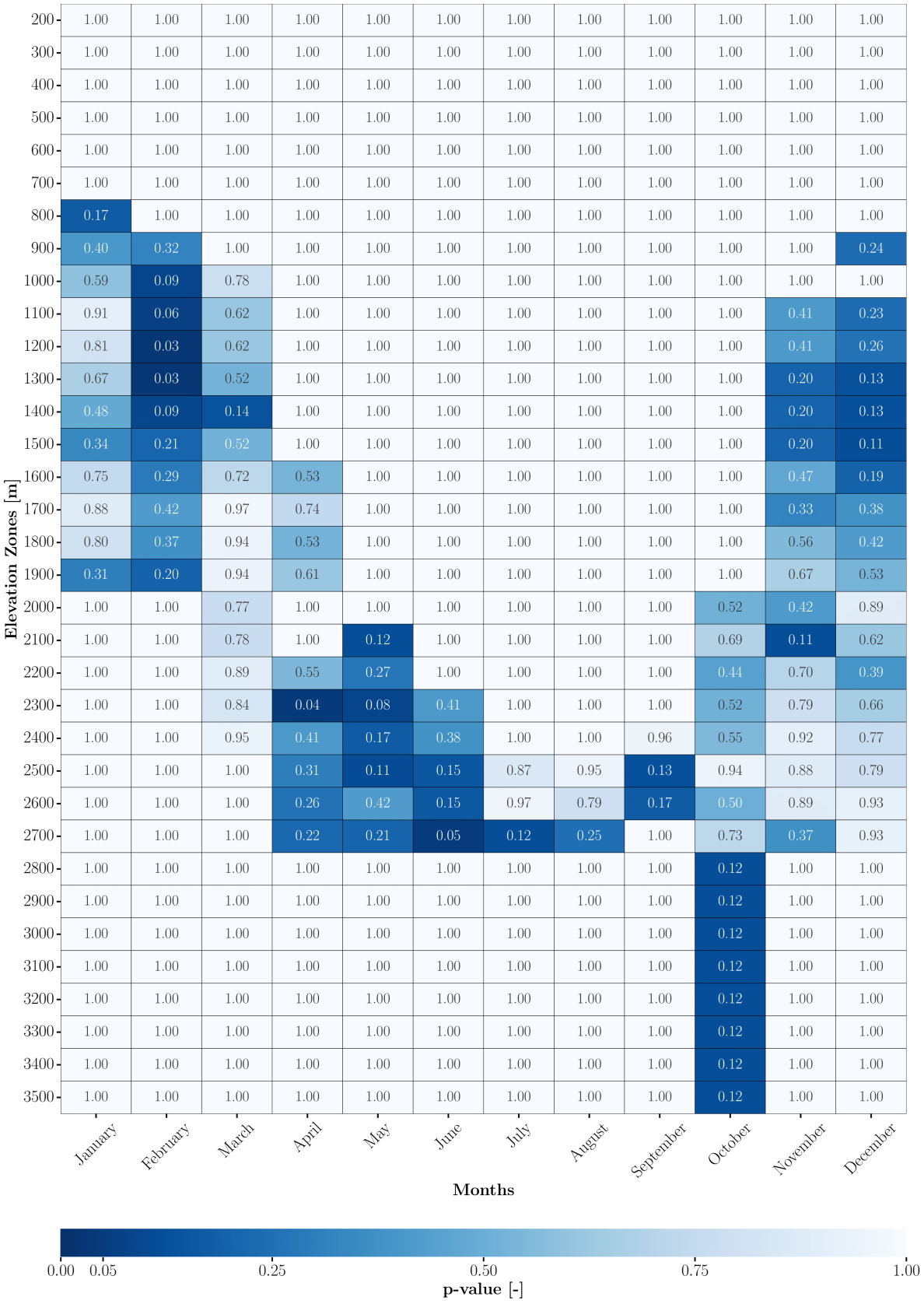

Figure 5.2: p-values of the Dsc trends for all elevation bands and all months

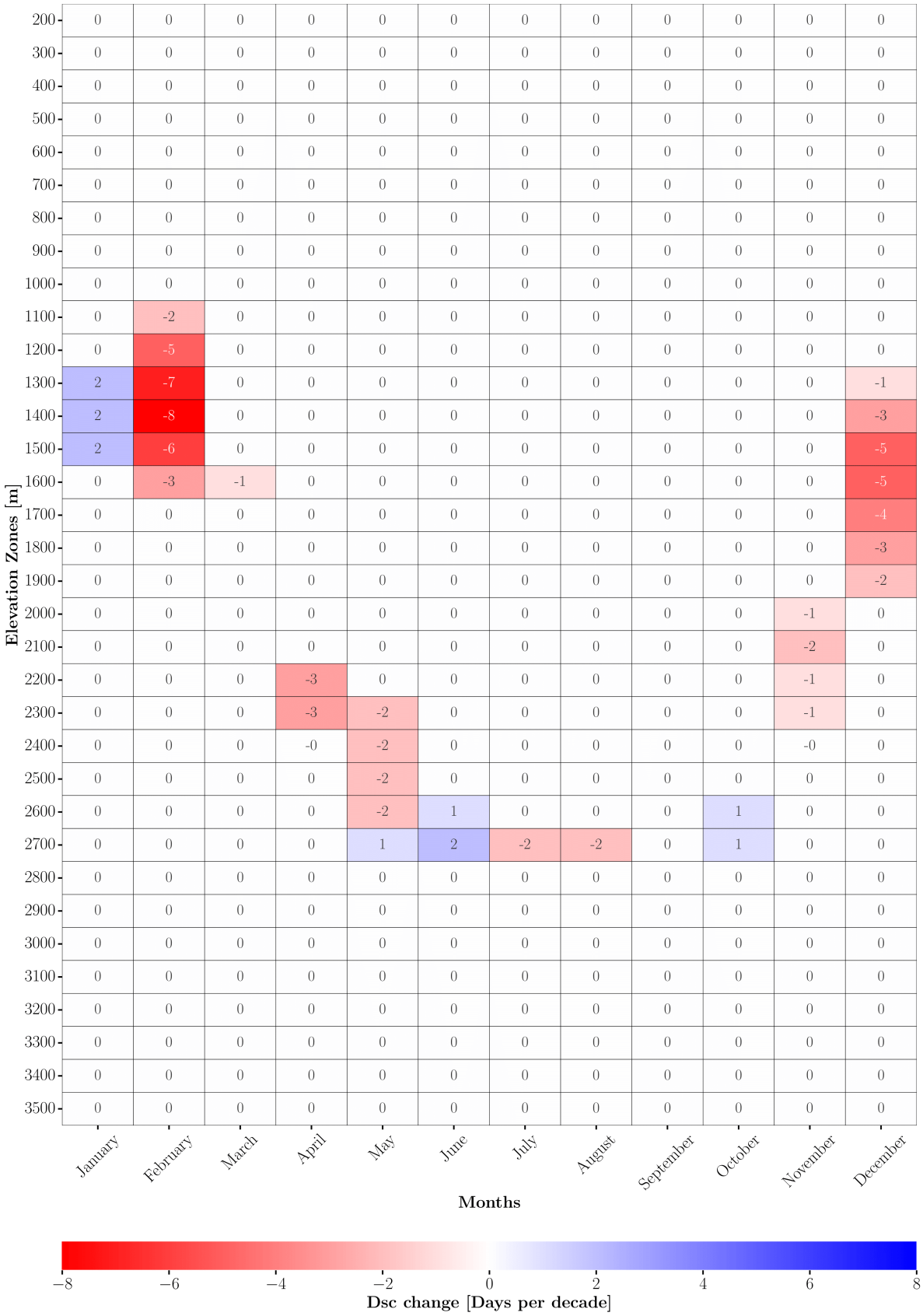

Figure 5.3: Change in the Dsc for all elevation bands and all months

From Figures 5.2 and 5.3 it is found that the lower p-values, i.e., the most significant trends, occur for the inter-annual trends of February's SCD at elevations around 1000 m - 1300 m. The estimated slope of these trends indicates a decrease of approximately 7 snow cover days per decade in February, at elevations of around 1000 m - 1300 m.

5.2. Monthly Regional Snowline Elevation (RSLE) for all sub-regions

In the following subsection, the trends in the monthly-averaged snowline elevation, for the different sub-regions and months, are investigated. The aim is to investigate the spatial patterns and the significance of the monthly-averaged snowline elevation.

Figure 5.4 presents the temporal variation of the median monthly-averaged regional snowline elevation across the years, for all months and sub-regions.

Figure 5.5 shows the calculated p-values for all months and sub-region of the Taurus mountain range. Lower p-values, which indicate more significant trends, are presented in a darker blue, and higher p-values are presented in lighter shades of blue. The white color is used for p-values equal to one.

Figure 5.6 presents the change, in meters per decade, in the median monthly-averaged snowline elevation for all months and sub-region of the Taurus mountain range.

Negative, i.e. downward, trends are illustrated with red colors, and positive, i.e. upward, trends are colored blue. For more substantial inter-annual changes in the RSLE, darker shades of blue and red are used for increasing and decreasing trends, respectively.

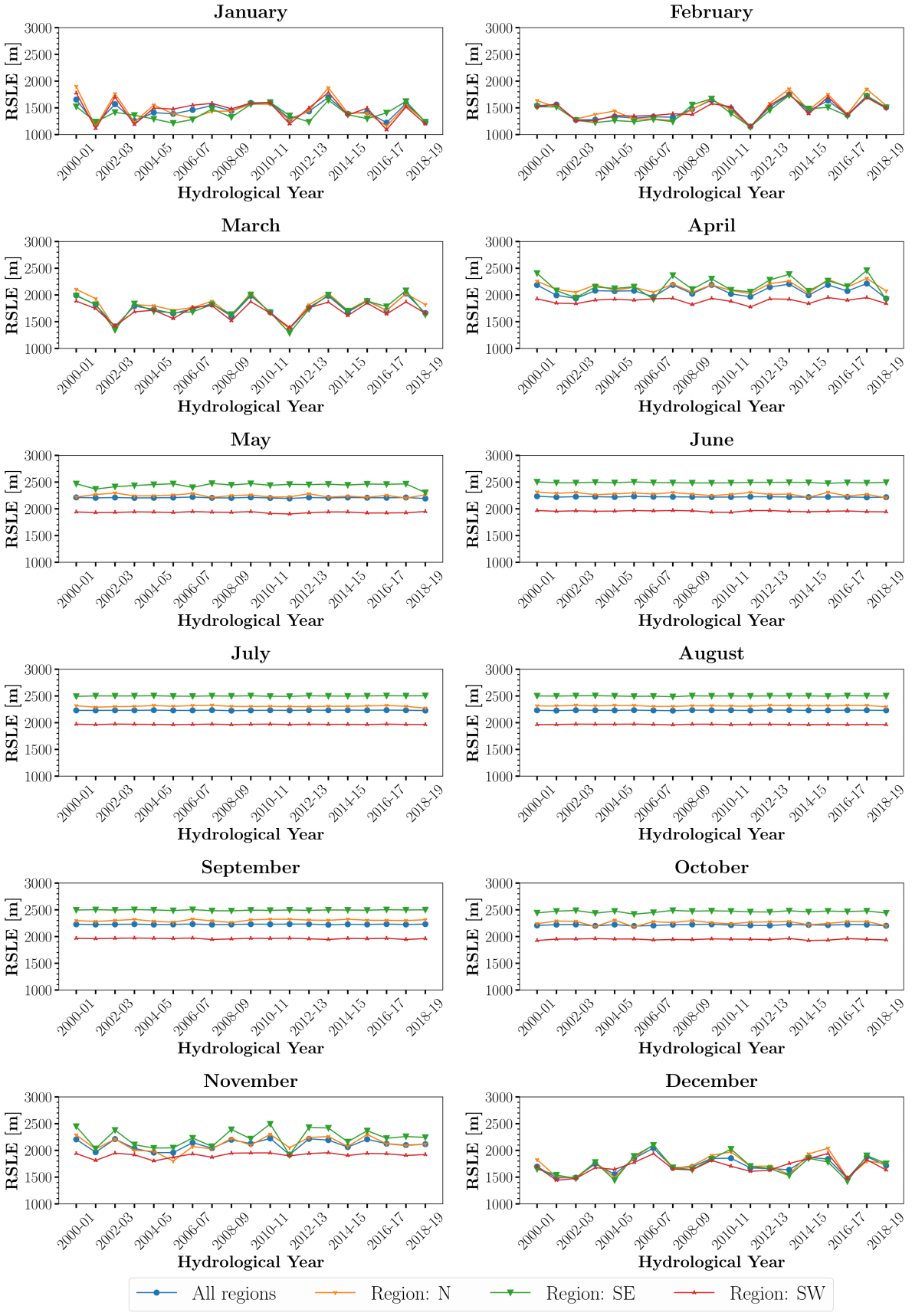

Figure 5.4: Median monthly regional snowline elevation from 2000 to 2019

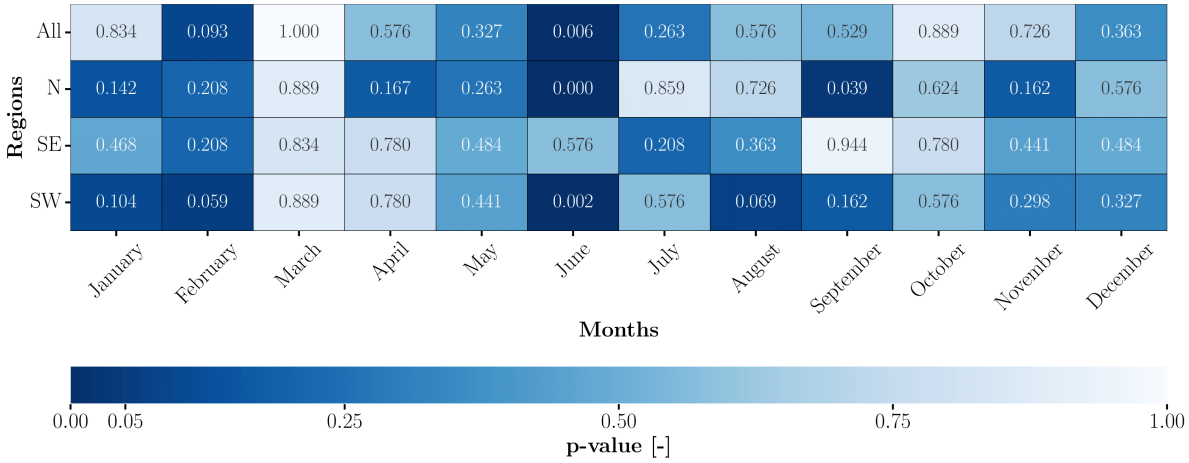

Figure 5.5: p-values of the median monthly RSLE trends for all months and sub-regions

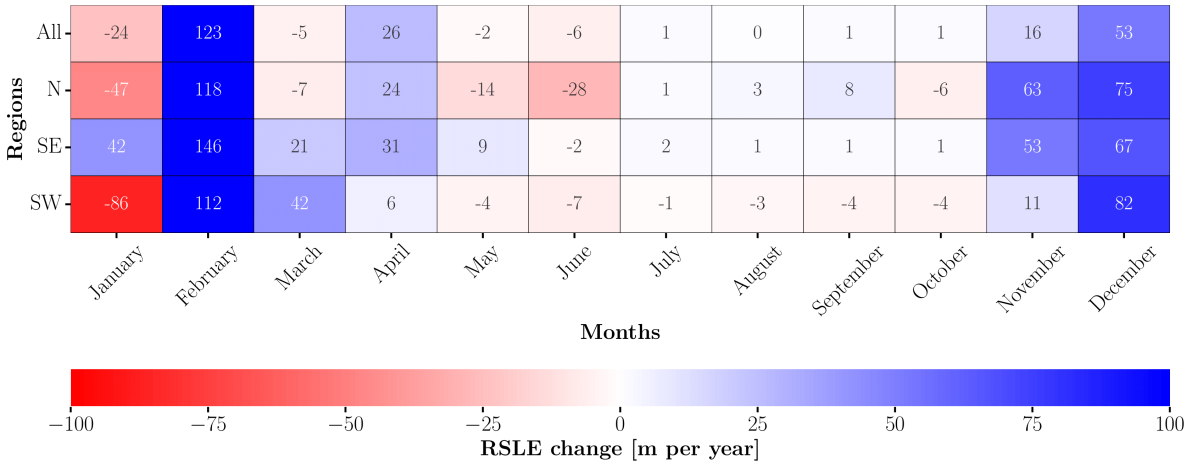

Figure 5.6: Change in the median monthly RSLE for all months and sub-regions

Due to the small number of ‘tiles’ used to extract the monthly averaged RSLE in the north (N) region, the results for that region are considered unreliable. Figures 5.5 and 5.6 indicate a decrease of 6 to 7 meters per decade in the RSLE in June for the whole TMR and especially in the southwestern (SW) region. This decrease is considered insignificant.

5.3. Daily median Regional Snowline Elevation (RSLE) for all sub-regions

In the following subsection, the trends in the daily RSLE are investigated for the different sub-regions.

The time series of the median daily RSLE are presented in Figure 5.7.

The results of the examination of the trends (see Section 4.2.7) of the four time series presented in Figure 5.7, are presented in Table 5.1.

Region	p-value [-]	Change [m/decade]
N	0.153	0.000
SE	0.012	0.015
SW	0.171	0.015
All regions	0.043	0.010

Table 5.1: Trend analysis of daily RSLE for the different sub-regions.

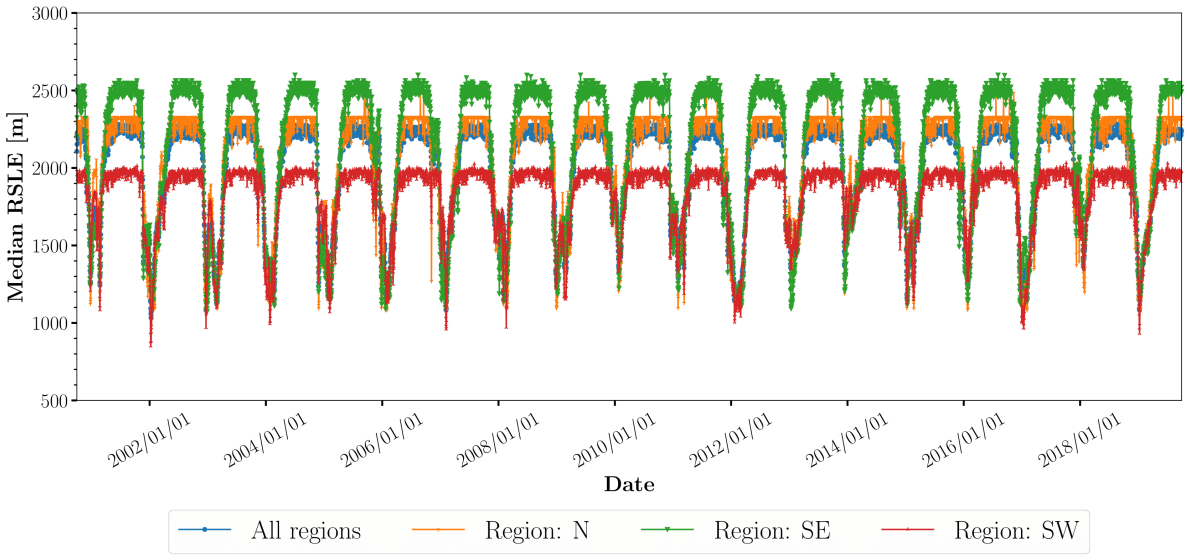

Figure 5.7: RSLE timeseries for all sub-regions

The modified MK test, to account for autocorrelation issues, is applied to the daily RLSE time series presented in Figure 5.7 but no notable changes were found.

5.4. Annual Number of Snow Cover Days (D_{SC}) examined across all sub-regions

In the following section, the results of analyzing the spatial and inter-annual variability of the annual number of snow cover days D_{SC} is examined. The spatial variability is examined in the sub-regions defined in Section 4.2.5 and the inter-annual variability is examined from 2000 to 2019.

Figure 5.8 consists of four sub-figures, each for a sub-region. Each sub-figure contains box-plots that illustrate the—average over each sub-region—annual number of snow cover days D_{SC} for all years from 2000 to 2019.

To analyze the inter-annual variability of the annual number of snow cover days (D_{SC}), the trends in the mean, median, 25th, and 75th percentiles of the box-plots presented in Figure 5.8 have been examined for all sub-regions.

Figure 5.9 illustrates the p-values of the aforementioned trends. Lower p-values indicate more significant upward or downward trends. Lower p-values are presented in a darker blue, and higher p-values are presented in a lighter blue, with p-values equal to one being presented with a white color.

Figure 5.10 illustrates the change, in days per decade, of the mean, median, 25th, and 75th percentiles of the annual number of snow cover days (D_{SC}) for all sub-regions. Negative and positive trends are colored red and blue, respectively. The more pronounced the change calculated using the Theil-Sein estimator, the darker the shade of the color.

The inter-annual variability of the annual number of snow cover days (D_{SC}) is examined for the whole TMR and the different sub-regions. No significant trends were observed in D_{SC} during the 2000-2019 period (see Figure 5.9).

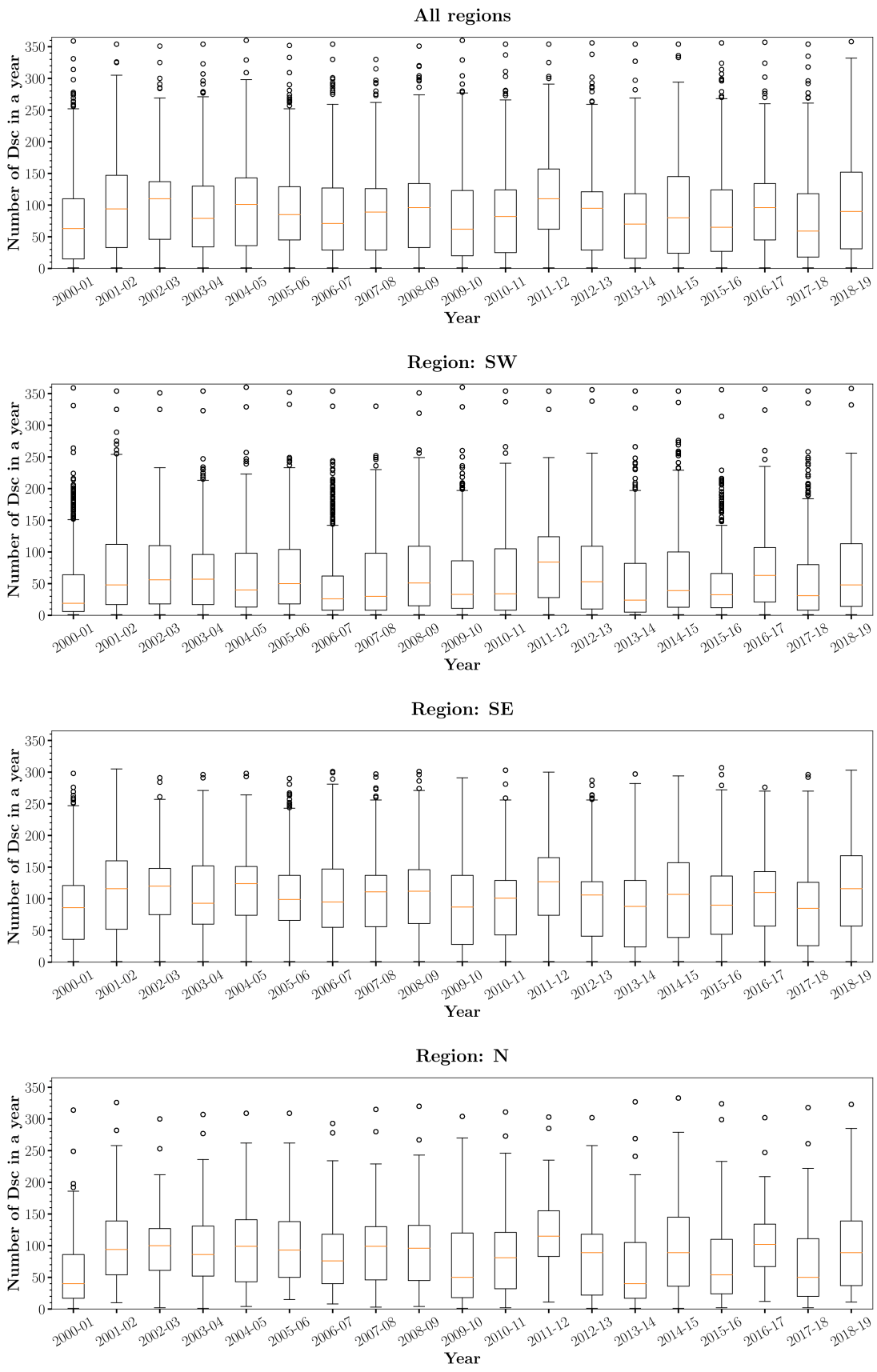

Figure 5.8: Annual number of snow covered days from 2000 to 2019 for all sub-regions

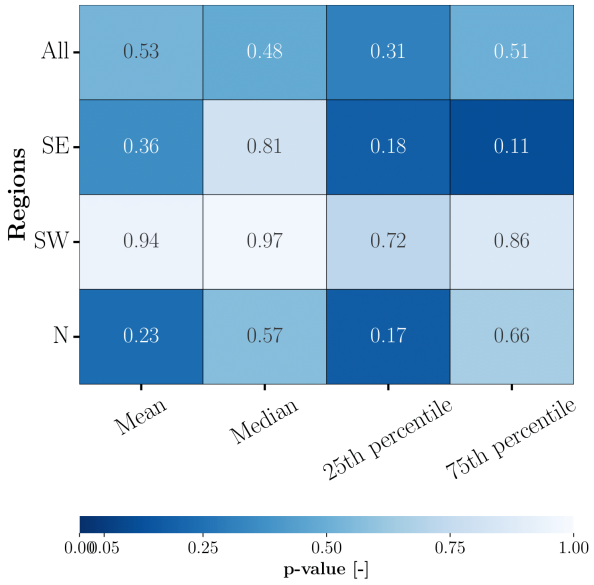

Figure 5.9: p-values of the trends in the mean, median, 25th and 75th percentiles of the annual number of snow covered days from 2000 to 2019 for all sub-regions

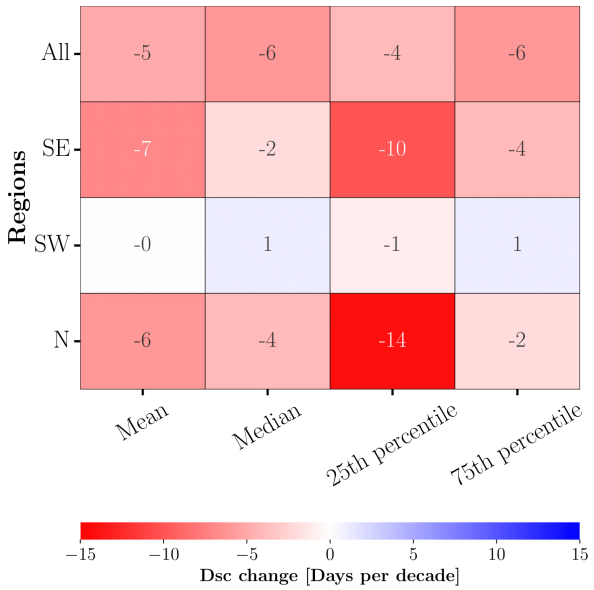

Figure 5.10: Change of the mean, median, 25th and 75th percentiles of the annual number of snow covered days from 2000 to 2019 for all sub-regions

5.5. Annual Number of Snow Cover Days (D_{SC}) examined across all elevation bands

In the following section, the results of analyzing the spatial and inter-annual variability of the annual number of snow cover days D_{SC} is examined. The spatial variability is examined in the 100-m elevation bands, and the inter-annual variability is examined from 2000 to 2019.

Figure 5.11 consists of four sub-figures, each for a sub-region. Each sub-figure contains box-plots for all elevation bands that present the annual number of snow cover days D_{SC}, considering all the years from 2000 to 2019.

Figure 5.12 is derived from Figure 5.11 and illustrates the median values of the annual number of snow covered days for all elevation bands and sub-regions.

Figure 5.13 illustrates the median annual number of snow cover days (D_{SC}) for all elevation bands, for the entire TMR, from 2000 to 2019.

Figure 5.14 shows the p-values (left sub-figure) and the slopes (right sub-figure) of the trends of the lines presented in Figure 5.13. In the left sub-figure, the lower the p-value, the more significant the upward or downward trend. Lower p-values are presented in a darker blue color, and higher p-values are presented in lighter shades, with p-values equal to one being presented with a white color. In the right sub-figure, the slope of the trends is presented in annual snow cover days per decade. Negative trends are colored red and positive trends are colored blue. The stronger the trends, the darker the shade of the color they have.

In Figure 5.14 it is shown that the most significant trends, i.e., lower p-values, are found when examining the inter-annual variability of D_{SC} at elevations between 2600 m and 3200 m throughout TMR. The estimated slope of these trends indicates a decrease of approximately 4 to 6 annual snow cover days per decade.

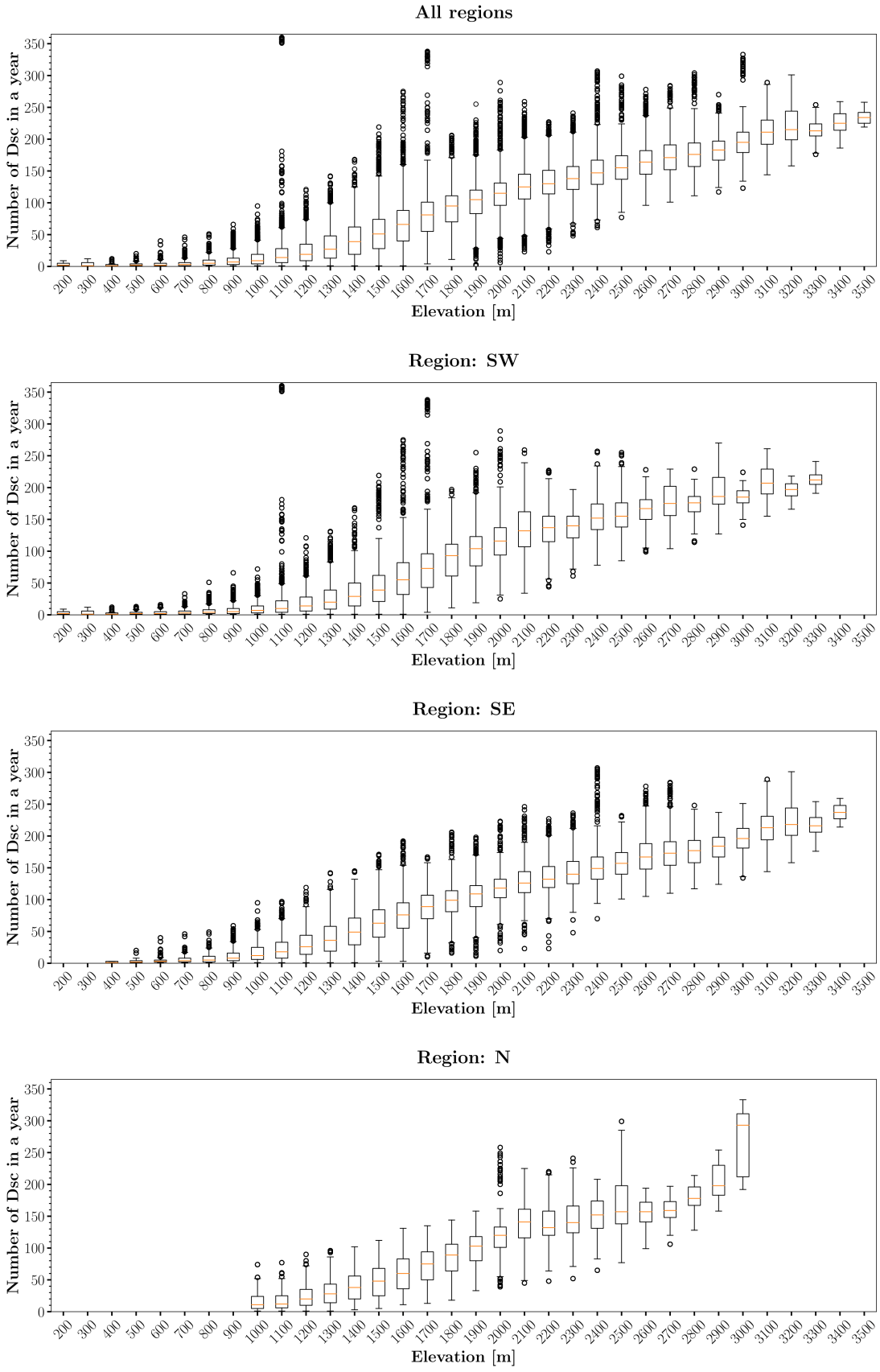

Figure 5.11: Annual Dsc for all elevation bands and sub-regions

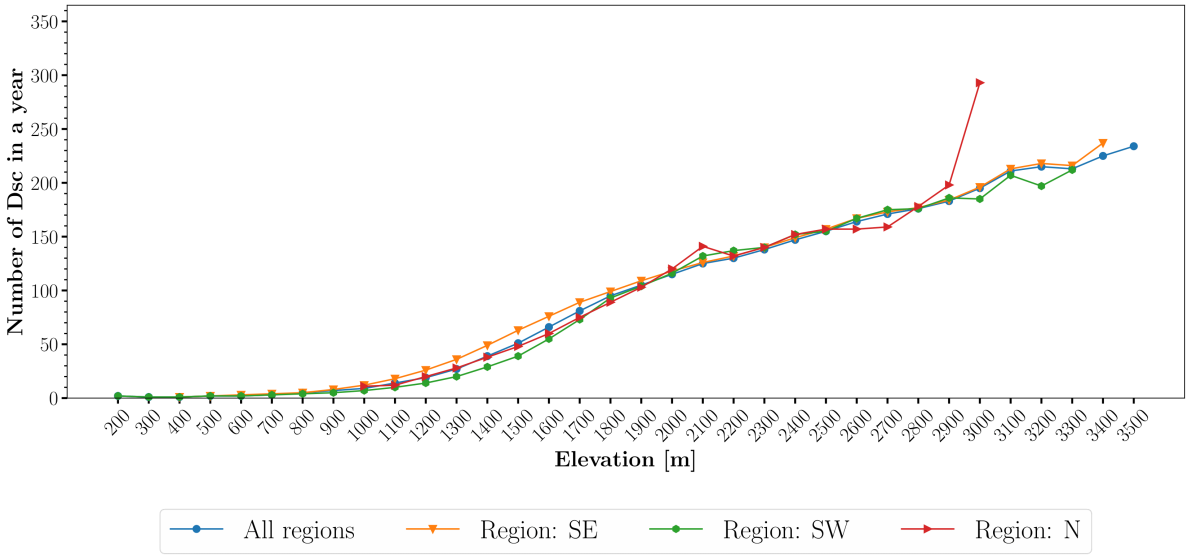

Figure 5.12: Median annual Dsc for all elevation bands and sub-regions

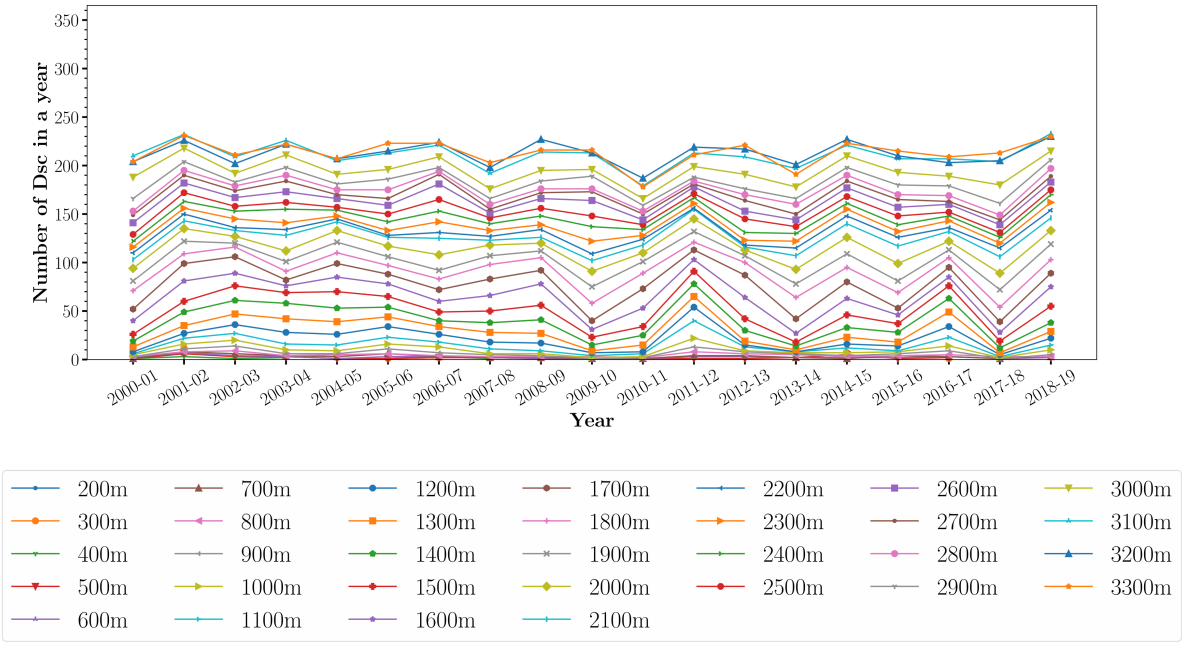

Figure 5.13: Annual number of snow covered days for all elevation bands,for the whole region, from 2000 to 2019

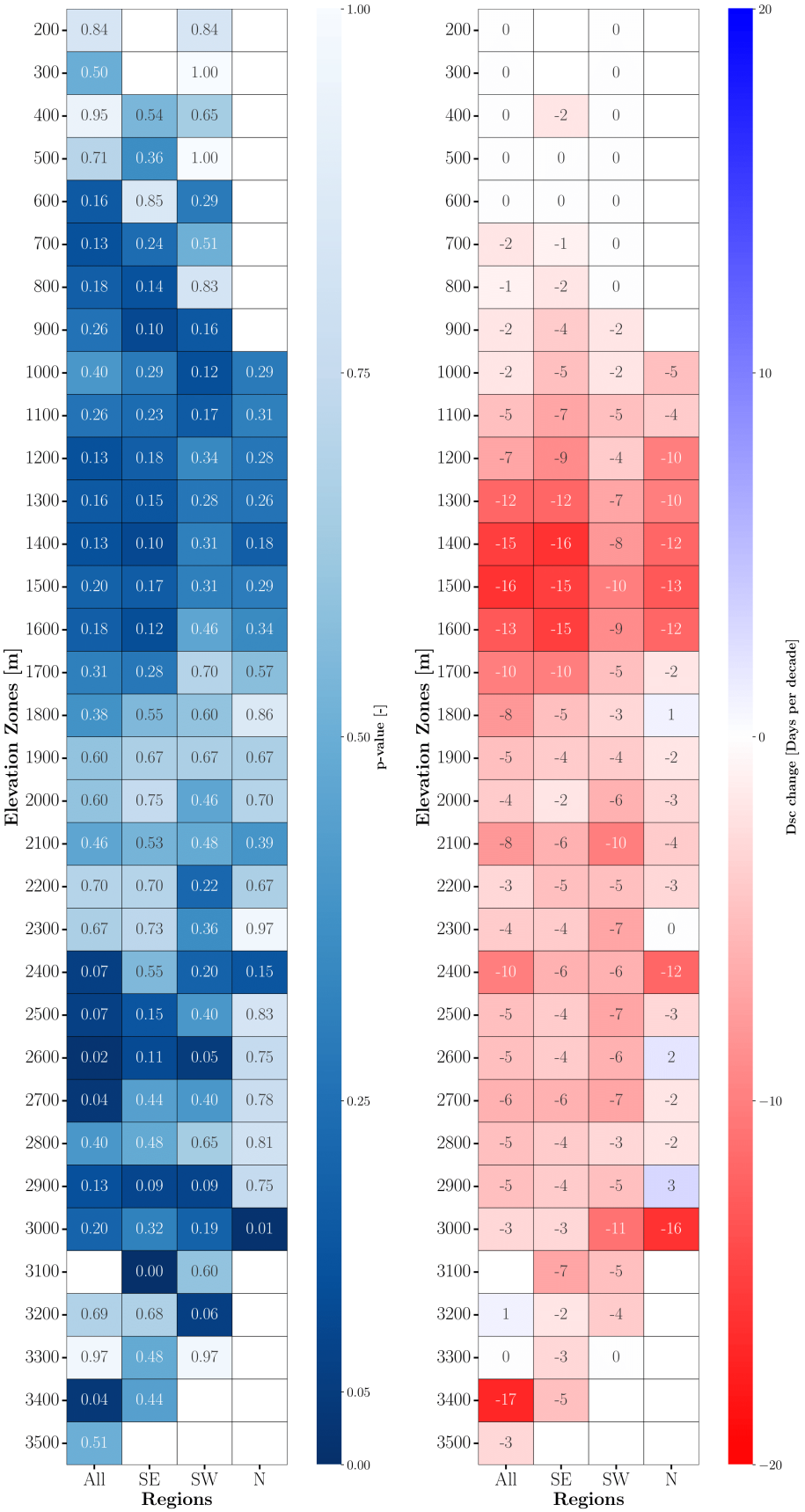

Figure 5.14: p-values and change per decade in the annual number of snow covered days for all elevation bands,for the whole region, from 2000 to 2019

5.6. Annual Number of Snow Cover Days (D_{SC}) examined across all 'tiles'

In the following section, the results of analyzing the spatial variability across the Taurus Mountain Range (TMR), by calculating D_{SC} for each 'tile', are analyzed.

Figure 5.15 presents a map showing the 19-year average of the annual number of snow cover days (D_{SC}) for all 'tiles' examined in the Taurus Mountains.

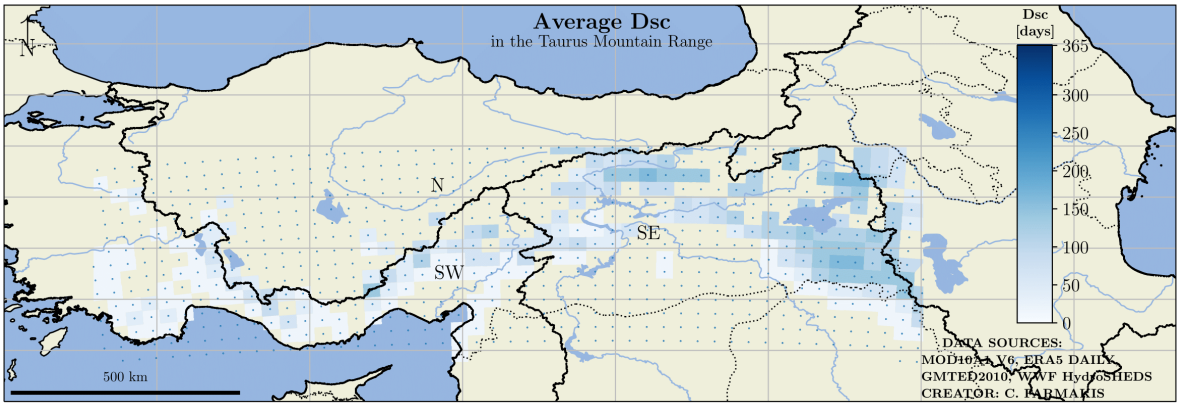

Figure 5.15: Average annual number of snow cover days throughout the Taurus mountains

The trends in the annual number of snow cover days (D_{SC}) have been examined for each 'tile' (see Section 4.2.7) and the map showing the average rate of change in D_{SC} across TMR is presented in Figure 5.16.

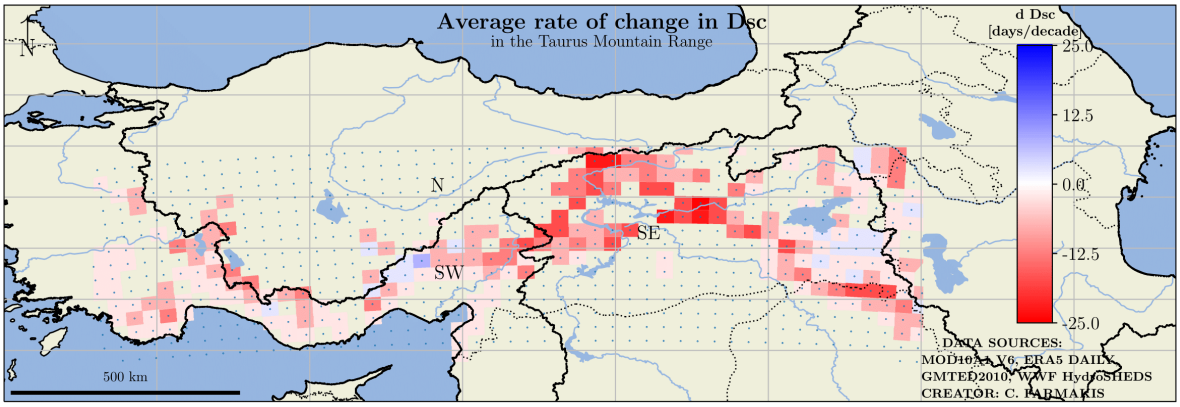

Figure 5.16: Average rate of change in the annual number of snow covered days throughout the Taurus mountains

Figure 5.17 presents the spatial coherence map, i.e, the p-values of the D_{SC} trends examined for all 'tiles', across TMR. The 'tiles' with p-values that correspond to the negative trends in D_{SC} are colored red, and the 'tiles' with p-values that correspond to the positive trends in D_{SC} are colored blue.

The 'tiles' with p values less than 0.05 are presented in Figure 5.18. The specific threshold, i.e. 0.5, is not of importance. The purpose of this analysis is to choose a low p-value to show the areas where significant changes in D_{SC} are found.

Figures 5.19 to 5.23 illustrate the average rate of change in the annual number of snow cover days (D_{SC}) for several elevation bands.

The spatial variability of D_{SC} across TMR is examined for all 'tiles' and is presented in Section 5.6. In general, no significant changes are observed in the annual number of snow cover days. There are few 'tiles' where the calculated trends are found to be significant (see Figure 5.18).

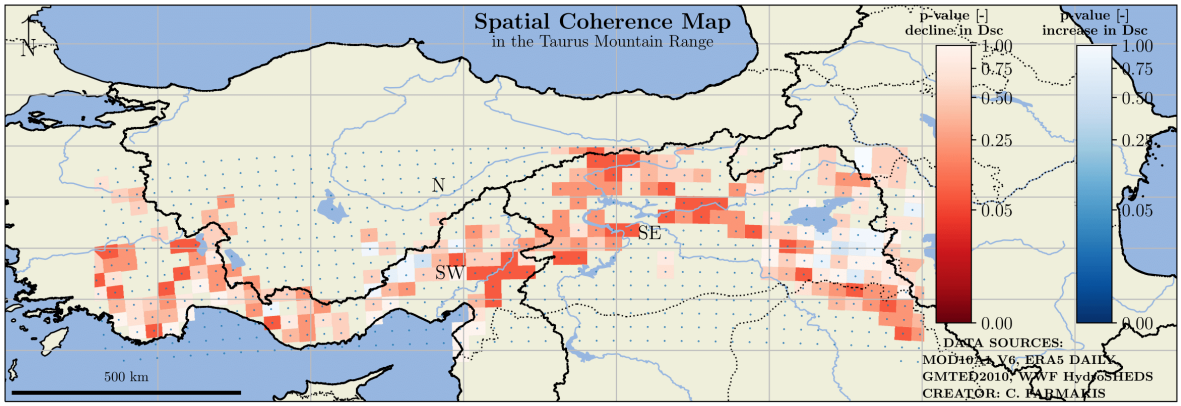

Figure 5.17: Spatial coherence map, p-values for increase (blue) and decrease (red) in the annual number of snow covered days

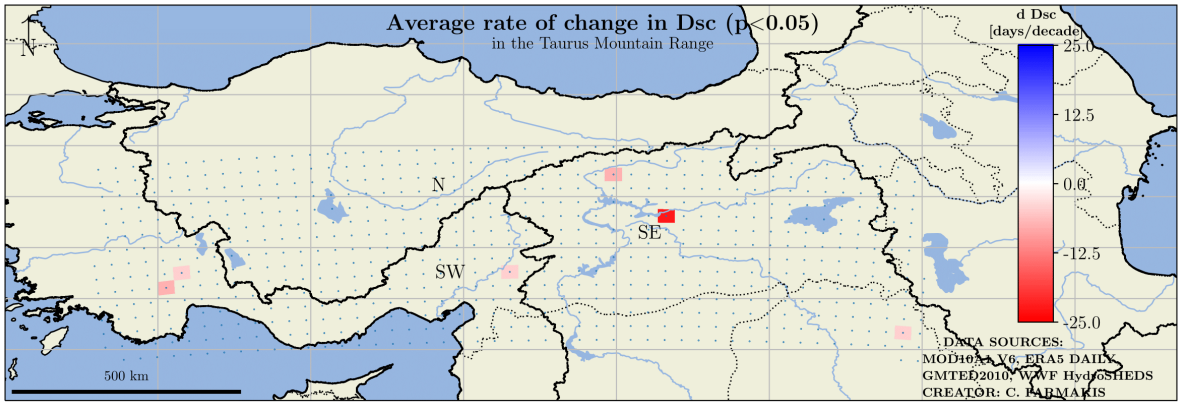

Figure 5.18: Average rate of change in the annual number of snow covered days throughout the Taurus mountains, for p-values lower than 0.05 (significant trends)

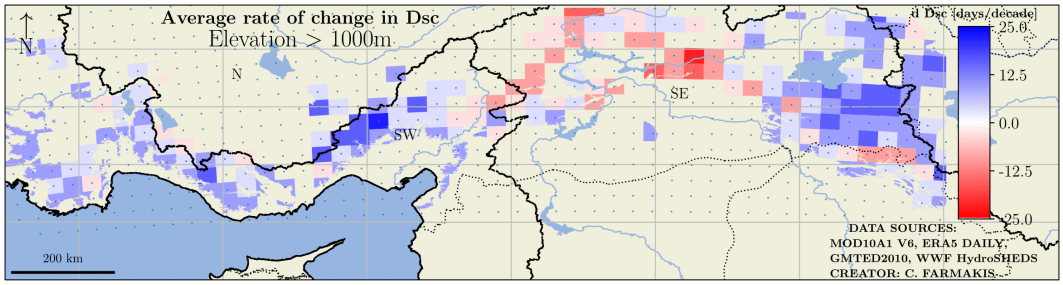

Figure 5.19: Average rate of change in the annual number of snow cover days D_{SC} for elevations greater than 1000 m.

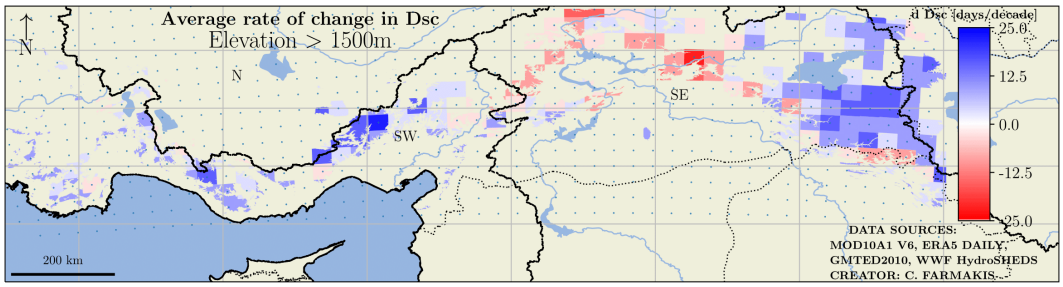

Figure 5.20: Average rate of change in the annual number of snow cover days D_{SC} for elevations greater than 1500 m.

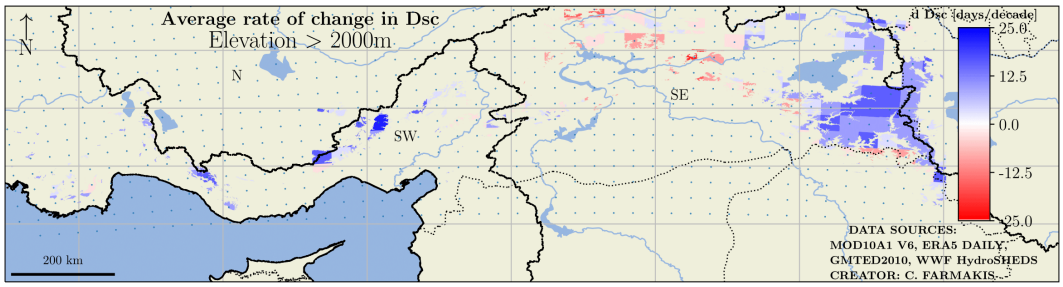

Figure 5.21: Average rate of change in the annual number of snow cover days D_{SC} for elevations greater than 2000 m.

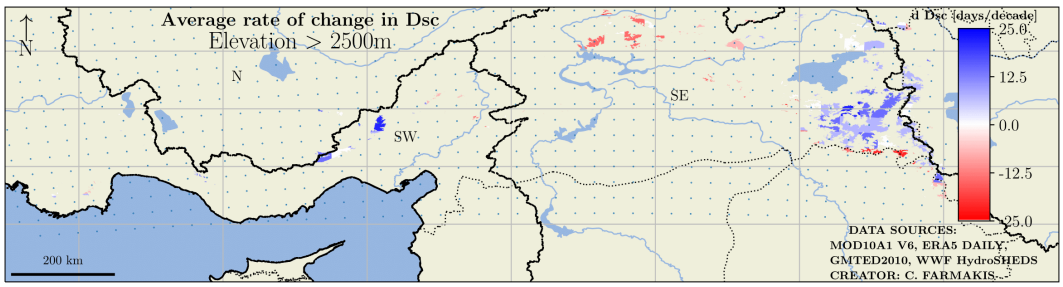

Figure 5.22: Average rate of change in the annual number of snow cover days D_{SC} for elevations greater than 2500 m.

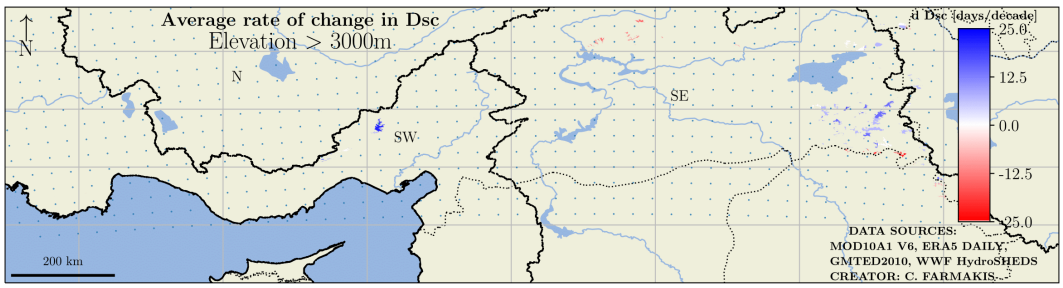

Figure 5.23: Average rate of change in the annual number of snow cover days D_{SC} for elevations greater than 3000 m.

5.7. Sensitivity of D_{SC} to inter-annual climatic variability

In the following chapter, the sensitivity of D_{SC} to inter-annual variability is examined using the first pair of climatic drivers presented in Section 4.2.8.

The two climatic drivers examined are the following:

1. Mean temperature for 6 months (November - April)
2. Total precipitation for 6 months (November - April)

The results of examining the sensitivity of the second pair of climatic drivers presented in Section 4.2.8 are found in Appendix B.

Figure 5.24 illustrates the adjusted R-squared values estimated for the different climatic drivers. The purpose of computing the adjusted R-squared values is to get an idea of the explanatory powers of the following:

1. the mean winter temperature Tw on D_{SC} (red boxes),
2. total winter precipitation Pw on D_{SC} (khaki boxes),
3. combined the aforementioned climatic drivers on D_{SC} (purple boxes).

The adjusted R-square was estimated using simple linear and multiple linear regression for each of the 100-m elevation bands in every sub-region.

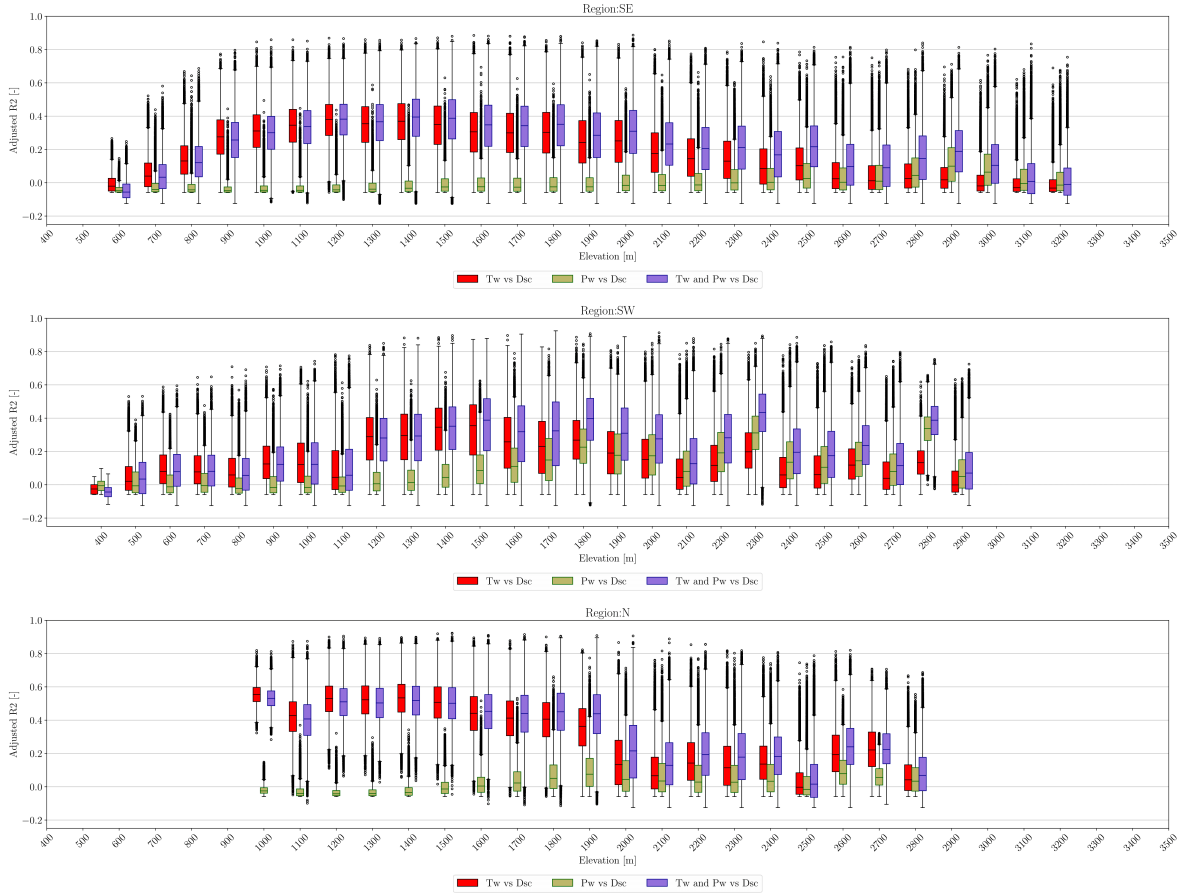

Figure 5.24: Explanatory powers of the different climatic drivers, i.e., Tw (red boxes), Pw (khaki boxes) and both of them (purple boxes), using the adjusted R-square.

Figure 5.25 presents the sensitivities of D_{SC} to total winter precipitation, for all elevation bands in every sub-region. Specifically, the figures show what the effect of a unit increase in total winter precipitation would be on the annual number of snow cover days (D_{SC}).

Similarly, Figure 5.26 illustrates the sensitivities of D_{SC} to mean winter temperature over the 2000-2019 period, for all 'tiles' in TMR.

Figures 5.27 and 5.28 present the sensitivities of D_{SC} to mean winter temperature over the 2000-2019 period, for all elevation bands in every sub-region (Figure 5.27) and for all 'tiles' in TMR (Figure 5.28).

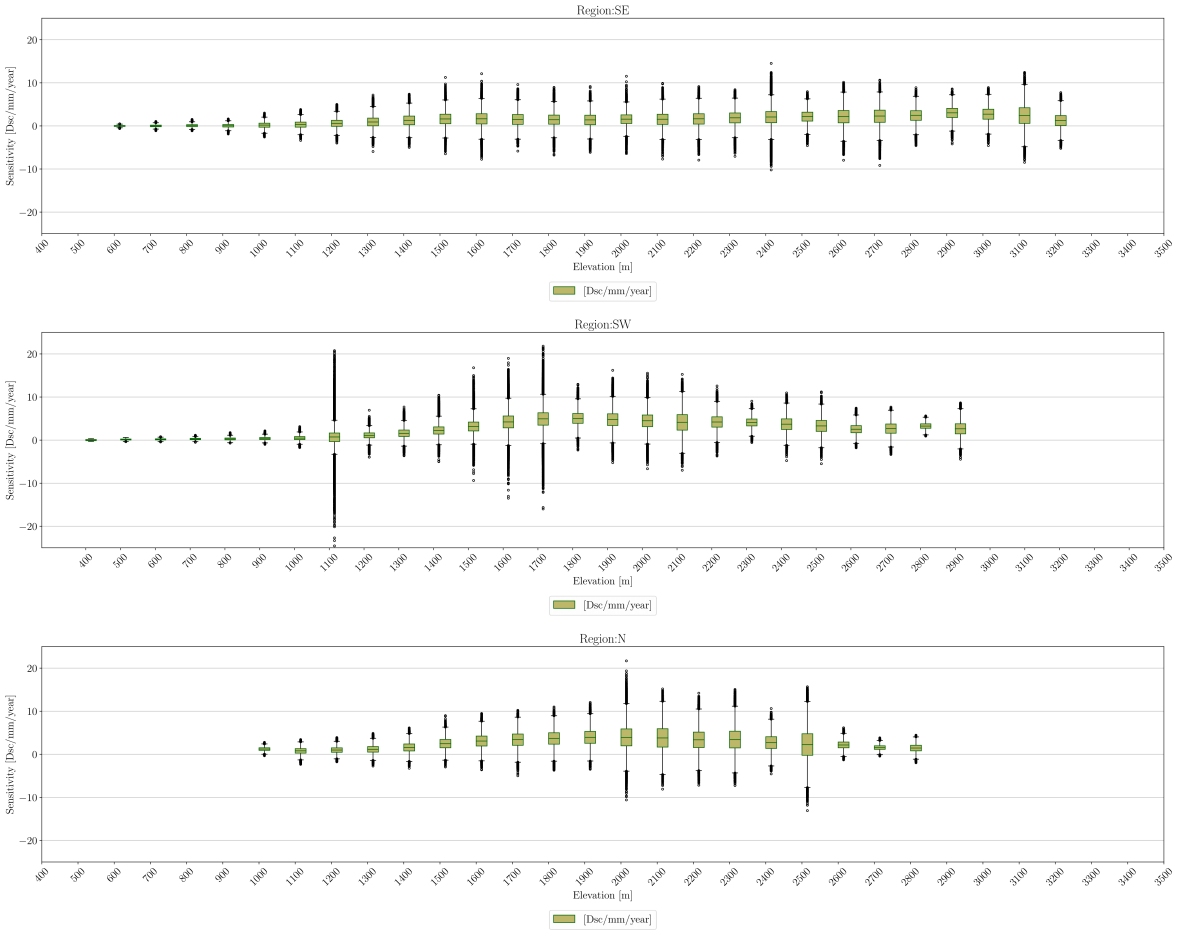

Figure 5.25: Sensitivities of D_{SC} to total winter precipitation (Pw), for all elevation bands in every sub-region.

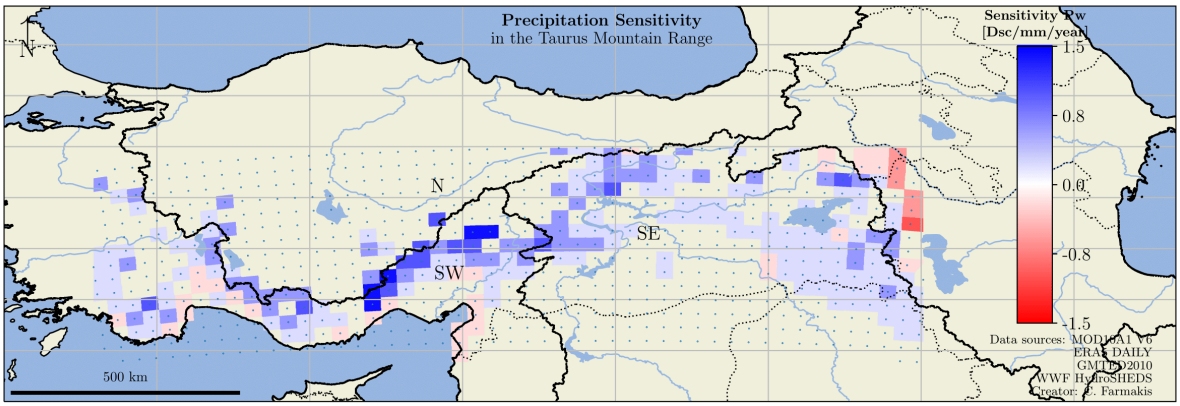

Figure 5.26: Sensitivities of D_{SC} to total winter precipitation (Pw), for all 'tiles' in TMR.

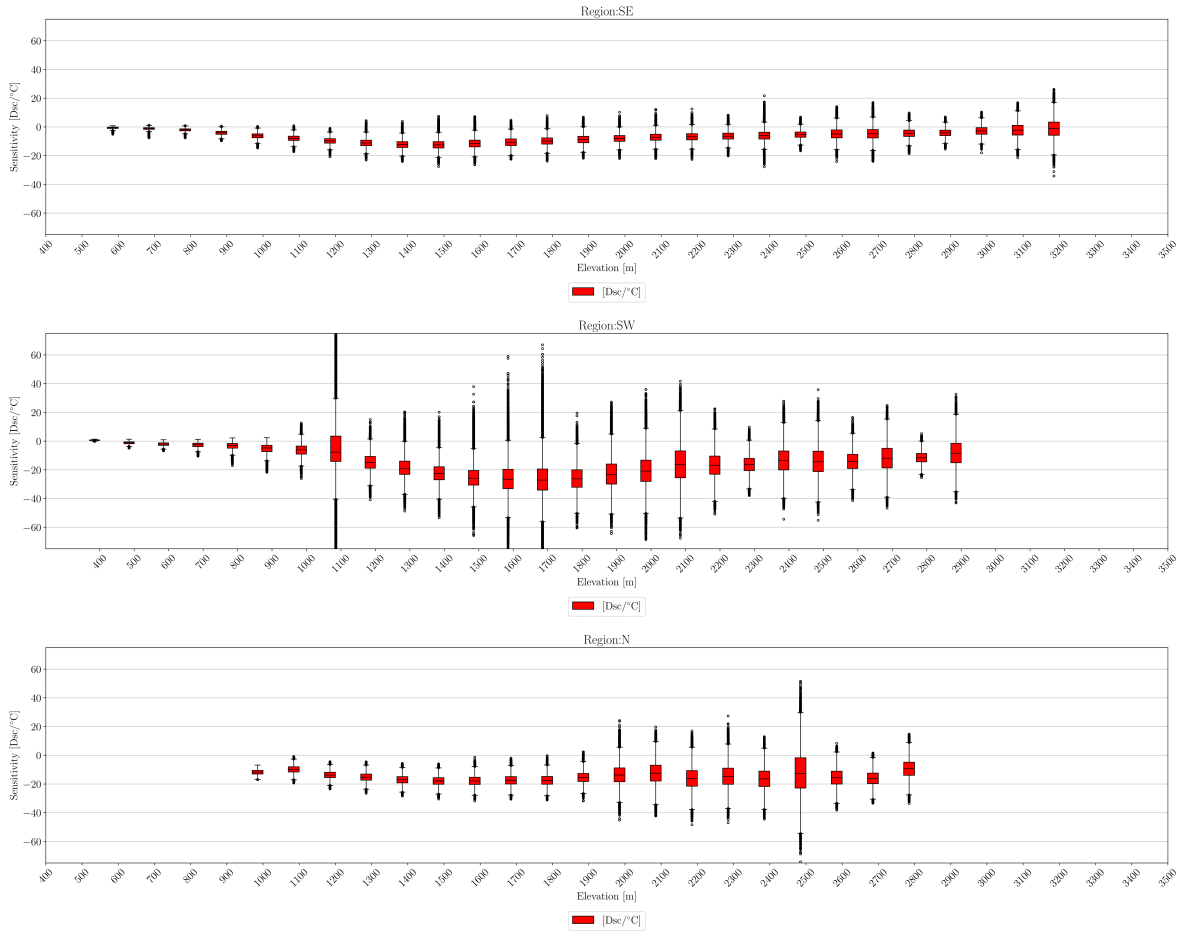

Figure 5.27: Sensitivities of D_{SC} to mean winter temperature (Tw), for all elevation bands in every sub-region.

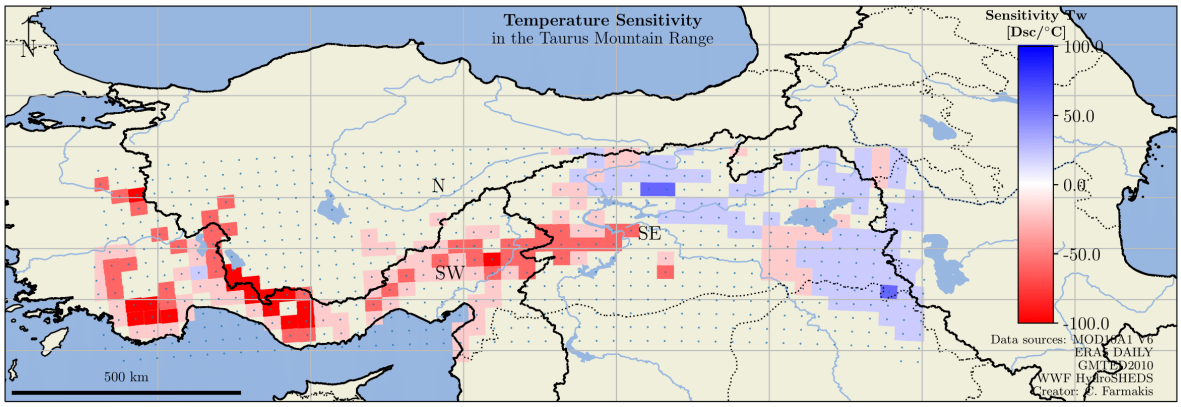

Figure 5.28: Sensitivities of D_{SC} to mean winter temperature (Tw), for all 'tiles' in TMR.

Investigating the sensitivity of D_{SC} to inter-annual climatic variability using mean winter temperature and precipitation results in the following conclusions:

- Winter temperature (Tw) is an important driver in the western Taurus Mountains for elevations above 1200 m, e.g., 1 degree Celsius increase in winter temperature would result in 20 D_{SC} less (see Figure 5.27).
- In the western Taurus Mountains an increase in average winter temperature (Tw) would result in a

decrease in D_{SC}, but in the eastern Taurus Mountains an increase in average winter temperature (Tw) would result in an increase in D_{SC} (see Figure 5.28).

- Winter precipitation (Pw) is an important driver in the western Taurus Mountains for elevations betwenn 1500 m and 2000 m, e.g., 1 mm increase in winter precipitation (November - April) would result in 5 D_{SC} less (see Figure 5.25).
- On the Mediterranean coast of Turkey and the eastern regions of TMR, an increase in winter precipitation (Pw) would result in a decrease in D_{SC}, but in all other areas, and especially in central TMR, an increase in winter precipitation (Pw) would result in an increase in D_{SC} (see Figure 5.26).

6

Limitations & uncertainties

In the following chapter, the limitations and uncertainties that affect the results of the analysis are presented. These uncertainties arise from the methods and data chosen and can be either the product of a choice made or intrinsic to the modeling process.

First, an important source of uncertainty is the snow cover product used.MOD10A1 V6 is a source of uncertainty because it marks pixels as snow covered or not based on an arbitrary choice of a threshold for NDSI. This approach might lead to systematic errors when calculating the Regional Snowline Elevation RSLE and the annual number of snow cover days D_{SC}.

Moreover, the method used to calculate the snowline elevation in the present analysis [16] has been developed for catchment scale studies but is used to calculate the snowline elevation on a larger—regional—scale. As a result, a suitable 'tile' size must be chosen to balance the spatial and temporal information availability. Investigating the appropriate 'tile' size is a time-consuming and computationally expensive process. In addition to the 'tile' size, the missing-pixel threshold must also be chosen. This choice determines the number of gaps in the RSLE time series and is responsible for systematic errors in the results of the analysis.

Another limitation of the current analysis is that there are no in situ snow measurements. In situ snow measurements would have been useful for a plausibility check of the snow cover cover results obtained using the RSLE method developed by Krajci et al. (2014).

In terms of the statistical analysis of the trends of D_{SC}, the 20-year period of the analysis is not sufficient to examine the long-term behavior of the duration and dynamics of snow cover in TMR. Remote-sensing snow cover studies are generally limited by the availability of data. A longer study period would have been needed, but this was not possible because there were no daily snow cover products available more than 20 years ago.

Finally, the sensitivity analysis performed to identify the climatic drivers of the duration of snow cover in the Taurus Mountains provides useful information across the Taurus Mountains, but since it follows a data-driven approach, it does not inform us of causality.

7

Conclusions & Recommendations

In the following chapter, the results of the analysis are summarized and recommendations for future research are provided.

7.1. Conclusions

In the analysis performed, the spatio-temporal patterns of the annual number of snow cover days (D_{SC}) across the TMR have been identified using the RSLE method developed by Krajci et al. (2014) and the modified Mann-Kendall (MK) non-parametric test [67] to examine trends in the annual and monthly number of snow cover days.

Very few results indicated changes in the patterns of snow cover duration. The most notable results were found at elevations between 2600 and 3200 m throughout the Taurus Mountains. At these elevations, a decrease of approximately five annual snow cover days (D_{SC}) per decade is found. Furthermore, a decrease of approximately 7 monthly snow cover days per decade is found for February at elevations of around 1000 m and 1300 m.

There are no further conclusions derived from examining trends in the annual number of snow cover days in the Taurus Mountains. This is a positive outcome that indicates that there are no significant future changes in snow cover patterns and, as a result, the availability of water in the region will not be at risk.

Additionally, the climatic drivers responsible for the variability of snow cover in the Taurus Mountain Range have been investigated. The climatic drivers examined are winter temperature, which is an important driver in the western Taurus Mountains for elevations above 1200 m, winter precipitation, which is an important driver in the western Taurus Mountains for elevations between 1500 m and 2000 m, solid precipitation, which is an important driver of snow cover throughout TMR for elevations around 1500 m, and the annual number of days with a mean temperature below zero, which is an important driver in the South West Taurus Mountains for elevations between 1500 m and 1800 m.

In general, the analysis carried out, considering the assumptions and limitations explained in Chapter 6, found that there is no reason to be concerned about future water shortages in the area of the Taurus Mountain Range due to the decrease in the water stored as snow.

7.2. Recommendations for future research

In the following section, some recommendations for future research on snow cover dynamics in the Taurus Mountains are provided.

In Chapter 6 it is mentioned that the method developed by Krajci et al. (2014) to calculate the Regional Snowline Elevation (RSLE) is suitable for catchment scale studies, and not for regional and global scale studies. As a result, the application of a more suitable method to calculate the snowline elevation could be beneficial to calculate the snowline elevation more accurately. This would result in a better estimate of the snow cover dynamics throughout the Taurus Mountain Range. In addition,in situ snow measurements would be useful for testing and evaluating the calculated regional snowline elevation using Krajci's method.

In the present research, the snow covered area is used as a snow metric to quantify seasonal snow dynamics across the Taurus Mountain Range. Snow covered area does not provide information on the water quantities stored in the snowpack, just the information that a certain area is covered or not with snow. As a result, a more hydrologically useful snow metric, such as the Snow Water Equivalent (SWE), would be beneficial to be used to examine snow dynamics across the Taurus Mountain Range.

Finally, the influence of exposure to solar radiation on snowline elevation can be examined. Solar radiation is an important driver of snow cover, and examining its influence on snow cover throughout the Taurus Mountains would provide useful information about its dynamics and future variability.

Bibliography

1. Musselman KN, Clark MP, Liu C, Ikeda K, and Rasmussen R. Slower snowmelt in a warmer world. Nature Climate Change 2017; 7:214–9. DOI: 10.1038/nclimate3225
2. Wang R, Nisoli C, Freitas R, Li J, McConville W, Cooley B, Lund M, Samarth N, Leighton C, Crespi V, et al. Artificial 'spin ice'in a geometrically frustrated lattice of nanoscale ferromagnetic islands. Nature 2006; 439:303–6
3. Madani K and Lund JR. Estimated impacts of climate warming on California's high-elevation hydropower. Climatic Change 2010; 102:521–38. DOI: 10.1007/s10584-009-9750-8
4. Mankin JS, Viviroli D, Singh D, Hoekstra AY, and Diffenbaugh NS. The potential for snow to supply human water demand in the present and future. Environmental Research Letters 2015 Nov; 10:114016. DOI: 10.1088/1748-9326/10/11/114016. Available from: https://doi.org/10.1088/1748-9326/10/11/114016
5. Hrachowitz M, Savenije H, Blöschl G, McDonnell J, Sivapalan M, Pomeroy J, Arheimer B, Blume T, Clark M, Ehret U, Fenicia F, Freer J, Gelfan A, Gupta H, Hughes D, Hut R, Montanari A, Pande S, Tetzlaff D, Troch P, Uhlenbrook S, Wagener T, Winsemius H, Woods R, Zehe E, and Cudennec C. A decade of Predictions in Ungauged Basins (PUB)—a review. Hydrological Sciences Journal 2013; 58:1198–255. DOI: 10.1080/02626667.2013.803183. eprint: https://doi.org/10.1080/02626667.2013.803183. Available from: https://doi.org/10.1080/02626667.2013.803183
6. Linderholm HW. Growing season changes in the last century. Agricultural and forest meteorology 2006; 137:1–14
7. Thackeray CW and Fletcher CG. Snow albedo feedback: Current knowledge, importance, outstanding issues and future directions. Progress in Physical Geography: Earth and Environment 2016; 40:392–408. DOI: 10.1177/0309133315620999. eprint: https://doi.org/10.1177/0309133315620999. Available from: https://doi.org/10.1177/0309133315620999
8. Hrachowitz M and Weiler M. Uncertainty of precipitation estimates caused by sparse gauging networks in a small, mountainous watershed. Journal of Hydrologic Engineering 2011; 16:460–71
9. Jonas T, Rixen C, Sturm M, and Stoeckli V. How alpine plant growth is linked to snow cover and climate variability. Journal of Geophysical Research: Biogeosciences 2008; 113
10. Hock R. A distributed temperature-index ice-and snowmelt model including potential direct solar radiation. Journal of glaciology 1999; 45:101–11
11. Mott R, Schirmer M, Bavay M, Grünewald T, and Lehning M. Understanding snow-transport processes shaping the mountain snow-cover. The Cryosphere 2010; 4:545–59
12. Dadic R, Mott R, Lehning M, and Burlando P. Wind influence on snow depth distribution and accumulation over glaciers. Journal of Geophysical Research: Earth Surface 2010; 115
13. DeBeer CM and Pomeroy JW. Influence of snowpack and melt energy heterogeneity on snow cover depletion and snowmelt runoff simulation in a cold mountain environment. Journal of hydrology 2017; 553:199–213
14. Mott R, Egli L, Grünewald T, Dawes N, Manes C, Bavay M, and Lehning M. Micrometeorological processes driving snow ablation in an Alpine catchment. The Cryosphere 2011; 5:1083–98
15. Grünewald T, Schirmer M, Mott R, and Lehning M. Spatial and temporal variability of snow depth and ablation rates in a small mountain catchment. The Cryosphere 2010; 4:215–25
16. Krajčí P, Holko L, Perdigão RA, and Parajka J. Estimation of regional snowline elevation (RSLE) from MODIS images for seasonally snow covered mountain basins. Journal of Hydrology 2014; 519:1769–78. DOI: https://doi.org/10.1016/j.jhydrol.2014.08.064. Available from: https://www.sciencedirect.com/science/article/pii/S0022169414007070

17. Da Ronco P and De Michele C. Cloud obstruction and snow cover in Alpine areas from MODIS products. Hydrology and earth system sciences 2014; 18:4579–600

18. Déry SJ and Brown RD. Recent Northern Hemisphere snow cover extent trends and implications for the snow-albedo feedback. Geophysical Research Letters 2007; 34. DOI: https://doi-org.tudelft.idm.oclc.org/10.1029/2007GL031474. eprint: https://agupubs-onlinelibrary-wiley-com.tudelft.idm.oclc.org/doi/pdf/10.1029/2007GL031474. Available from: https://agupubs-onlinelibrary-wiley-com.tudelft.idm.oclc.org/doi/abs/10.1029/2007GL031474

19. Hori M, Sugiura K, Kobayashi K, Aoki T, Tanikawa T, Kuchiki K, Niwano M, and Enomoto H. A 38-year (1978–2015) Northern Hemisphere daily snow cover extent product derived using consistent objective criteria from satellite-borne optical sensors. Remote Sensing of Environment 2017; 191:402–18. DOI: https://doi.org/10.1016/j.rse.2017.01.023. Available from: https://www.sciencedirect.com/science/article/pii/S0034425717300342

20. Robinson DA. Monitoring northern hemisphere snow cover. Glaciol. Data Rep. 1993; 25:1–25

21. Hrachowitz M and Clark MP. HESS Opinions: The complementary merits of competing modelling philosophies in hydrology. Hydrology and Earth System Sciences 2017; 21:3953–73. DOI: https://doi.org/10.5194/hess-21-3953-2017

22. Beven K. On undermining the science? Hydrological Processes 2006; 20:3141–6. DOI: https://doi-org.tudelft.idm.oclc.org/10.1002/hyp.6396. eprint: https://onlinelibrary-wiley-com.tudelft.idm.oclc.org/doi/pdf/10.1002/hyp.6396. Available from: https://onlinelibrary-wiley-com.tudelft.idm.oclc.org/doi/abs/10.1002/hyp.6396

23. Gafurov A and Bárdossy A. Cloud removal methodology from MODIS snow cover product. Hydrology and Earth System Sciences 2009; 13:1361–73. DOI: 10.5194/hess-13-1361-2009. Available from: https://hess.copernicus.org/articles/13/1361/2009/

24. Deems JS, Painter TH, and Finnegan DC. Lidar measurement of snow depth: a review. Journal of Glaciology 2013; 59:467–79

25. Kunkel KE, Robinson DA, Champion S, Yin X, Estilow T, and Frankson RM. Trends and extremes in Northern Hemisphere snow characteristics. Current Climate Change Reports 2016; 2:65–73

26. Fontrodona Bach A, Van der Schrier G, Melsen L, Klein Tank A, and Teuling A. Widespread and accelerated decrease of observed mean and extreme snow depth over Europe. Geophysical Research Letters 2018; 45:12–312

27. Brown RD and Robinson DA. Northern Hemisphere spring snow cover variability and change over 1922–2010 including an assessment of uncertainty. The Cryosphere 2011; 5:219–29

28. Hernández-Henríquez MA, Déry SJ, and Derksen C. Polar amplification and elevation-dependence in trends of Northern Hemisphere snow cover extent, 1971–2014. Environmental Research Letters 2015; 10:044010

29. Mudryk L, Kushner P, Derksen C, and Thackeray C. Snow cover response to temperature in observational and climate model ensembles. Geophysical Research Letters 2017; 44:919–26

30. Hantel M, Ehrendorfer M, and Haslinger A. Climate sensitivity of snow cover duration in Austria. International Journal of Climatology: A Journal of the Royal Meteorological Society 2000; 20:615–40

31. Hammond JC, Saavedra FA, and Kampf SK. Global snow zone maps and trends in snow persistence 2001–2016. International Journal of Climatology 2018; 38:4369–83

32. Parajka J and Blöschl G. Validation of MODIS snow cover images over Austria. Hydrology and Earth System Sciences 2006; 10:679–89. DOI: 10.5194/hess-10-679-2006. Available from: https://hess.copernicus.org/articles/10/679/2006/

33. Immerzeel WW, Droogers P, De Jong S, and Bierkens M. Large-scale monitoring of snow cover and runoff simulation in Himalayan river basins using remote sensing. Remote sensing of Environment 2009; 113:40–9

34. Brown RD and Mote PW. The response of Northern Hemisphere snow cover to a changing climate. Journal of Climate 2009; 22:2124–45
35. Allchin MI and Déry SJ. A spatio-temporal analysis of trends in Northern Hemisphere snow-dominated area and duration, 1971–2014. Annals of Glaciology 2017; 58:21–35
36. Tang BH, Shrestha B, Li ZL, Liu G, Ouyang H, Gurung DR, Giriraj A, and San Aung K. Determination of snow cover from MODIS data for the Tibetan Plateau region. International Journal of Applied Earth Observation and Geoinformation 2013; 21:356–65
37. Rittger K, Painter TH, and Dozier J. Assessment of methods for mapping snow cover from MODIS. Advances in Water Resources 2013; 51:367–80
38. Gascoin S, Hagolle O, Huc M, Jarlan L, Dejoux JF, Szczypta C, Marti R, and Sánchez R. A snow cover climatology for the Pyrenees from MODIS snow products. Hydrology and Earth System Sciences 2015; 19:2337–51. DOI: 10.5194/hess-19-2337-2015. Available from: https://hess.copernicus.org/articles/19/2337/2015/
39. Durand Y, Giraud G, Laternser M, Etchevers P, Mérindol L, and Lesaffre B. eanalysis of 47 Years of Climate in the French Alps (1958–2005): Climatology and Trends for Snow Cover. Journal of Applied Meteorology and Climatology 2009; 48:2487–512. DOI: 10.1175/2009JAMC1810.1. Available from: https://journals.ametsoc.org/view/journals/apme/48/12/2009jamc1810.1.xml
40. Marke T, Strasser U, Hanzer F, Stötter J, Wilcke RAI, and Gobiet A. Scenarios of future snow conditions in Styria (Austrian Alps). Journal of Hydrometeorology 2015; 16:261–77
41. Schmucki E, Marty C, Fierz C, and Lehning M. Simulations of 21st century snow response to climate change in Switzerland from a set of RCMs. International journal of climatology 2015; 35:3262–73
42. Gorelick N, Hancher M, Dixon M, Ilyushchenko S, Thau D, and Moore R. Google Earth Engine: Planetary-scale geospatial analysis for everyone. Remote sensing of Environment 2017; 202:18–27
43. Britannica TEoE. Taurus Mountains. Encyclopedia Britannica. 2014 Apr 15. Available from: https://www.britannica.com/place/Taurus-Mountains
44. Wikipedia contributors. Taurus Mountains — Wikipedia, The Free Encyclopedia. [Online; accessed 23-May-2022]. 2022. Available from: https://https://en.wikipedia.org/wiki/Taurus_Mountains
45. Green AR. The storm-god in the ancient Near East. Penn State Press, 2003
46. Painter TH, Rittger K, McKenzie C, Slaughter P, Davis RE, and Dozier J. Retrieval of subpixel snow covered area, grain size, and albedo from MODIS. Remote Sensing of Environment 2009; 113:868–79
47. Stehr A and Aguayo M. Snow cover dynamics in Andean watersheds of Chile (32.0–39.5 S) during the years 2000–2016. Hydrology and Earth System Sciences 2017; 21:5111–26
48. Redpath TA, Sirguey P, and Cullen NJ. Characterising spatio-temporal variability in seasonal snow cover at a regional scale from MODIS data: The Clutha Catchment, New Zealand. Hydrology and Earth System Sciences 2019; 23:3189–217
49. Wikipedia contributors. Terra (satellite) — Wikipedia, The Free Encyclopedia. [Online; accessed 2-June-2022]. 2022. Available from: https://en.wikipedia.org/wiki/Terra_(satellite)
50. Danielson JJ and Gesch DB. Global multi-resolution terrain elevation data 2010 (GMTED2010). 2011. DOI: 10.3133/ofr20111073
51. Farr TG and Kobrick M. Shuttle Radar Topography Mission produces a wealth of data. Eos, Transactions American Geophysical Union 2000; 81:583–5
52. (CDS) CCCSCDS. Copernicus Climate Change Service (C3 S)(2017): ERA5: Fifth generation of ECMWF atmospheric reanalyses of the global climate. 2017
53. Muñoz-Sabater J, Dutra E, Agustí-Panareda A, Albergel C, Arduini G, Balsamo G, Boussetta S, Choulga M, Harrigan S, Hersbach H, et al. ERA5-Land: A state-of-the-art global reanalysis dataset for land applications. Earth System Science Data 2021; 13:4349–83

54. Lehner B, Verdin K, and Jarvis A. New global hydrography derived from spaceborne elevation data. Eos, Transactions American Geophysical Union 2008; 89:93–4. DOI: 10.1029/2008EO100001

55. Lehner B and Grill G. Global river hydrography and network routing: baseline data and new approaches to study the world's large river systems. Hydrological Processes 2013; 27:2171–86. DOI: 10.1002/hyp.9740

56. Köppen W. Die Wärmezonen der Erde, nach der Dauer der heissen, gemässigten und kalten Zeit und nach der Wirkung der Wärme auf die organische Welt betrachtet. Meteorologische Zeitschrift 1884; 1:5–226

57. Koppen W. Das geographische system der klimat. Handbuch der klimatologie 1936 :46

58. Koppen W. Klassification der Klimate nach Temperatur, Niedenschlag und Jahreslauf. Petermanns Geogr. Mitt. 1918; 64:193–203

59. Geiger R and Pohl W. Eine neue Wandkarte der Klimagebiete der Erde nach W. Köppens Klassifikation (A New Wall Map of the Climatic Regions of the World According to W. Köppen's Classification). Erdkunde 1954 :58–61

60. Geiger R. Das klima der bodennahen luftschicht. Anzeiger für Schädlingskunde 1961; 34:159–9

61. Esch T van. Estimating snow cover decline using the RSLE in Google Earth Engine: A Caucasus case study. 2019. Available from: http://resolver.tudelft.nl/uuid:196d467a-f0ae-480d-a3e3-d2da97e821bc

62. Lehner B and Grill G. Global river hydrography and network routing: baseline data and new approaches to study the world's large river systems. Hydrological Processes 2013; 27:2171–86

63. Köppen W and Geiger R. Handbuch der klimatologie. Vol. 1. Gebrüder Borntraeger Berlin, 1930

64. Beck HE, Zimmermann NE, McVicar TR, Vergopolan N, Berg A, and Wood EF. Present and future Köppen-Geiger climate classification maps at 1-km resolution. Scientific data 2018; 5:1–12

65. Theil H. A rank-invariant method of linear and polynomial regression analysis. Indagationes mathematicae 1950; 12:173

66. Theil H. Economic forecasts and policy. 1961

67. Hamed KH and Ramachandra Rao A. A modified Mann-Kendall trend test for autocorrelated data. Journal of Hydrology 1998; 204:182–96. DOI: https://doi.org/10.1016/S0022-1694(97)00125-X. Available from: https://www.sciencedirect.com/science/article/pii/S002216949700125X

68. Liu Q. Spatiotemporal snow pattern in the Qilian Mountains from 2001 to 2018. 2020. Available from: http://resolver.tudelft.nl/uuid:a5f5c933-a7b9-4a64-88b6-2c2752208150

Appendix A

In the following chapter, some results of the analysis (maps) derived from choosing different ‘tile’ sizes, i.e., 30 km and 50 km, are presented (Table A.1).

	‘Tile’ size: 30 km.	‘Tile’ size: 50 km
1	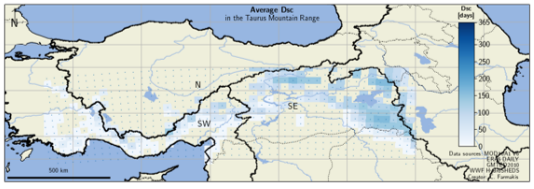	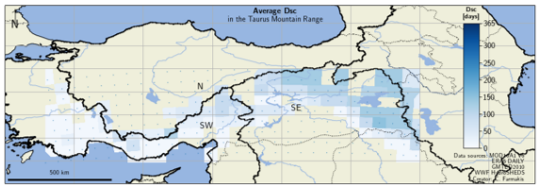
2	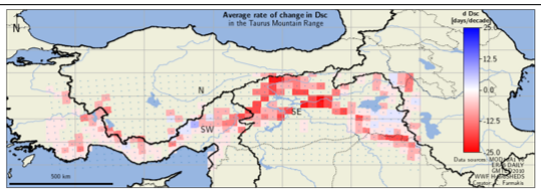	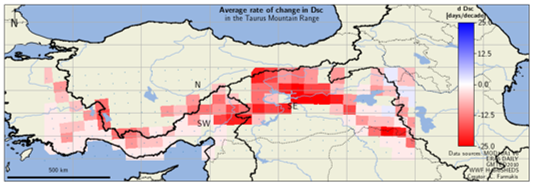
3	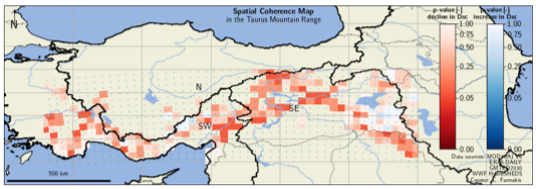	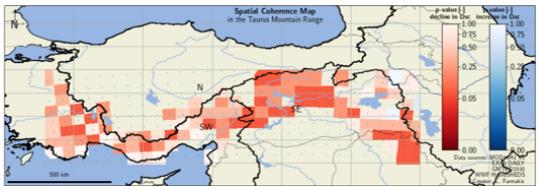
4	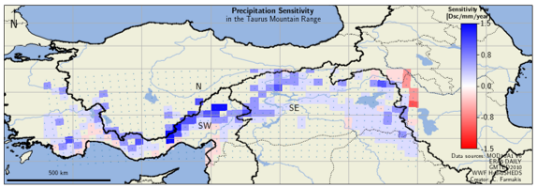	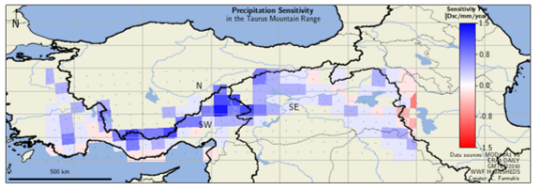
5	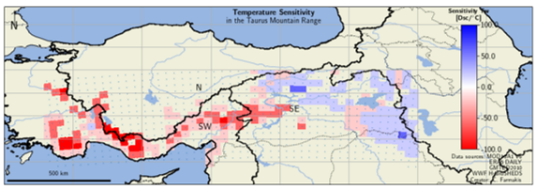	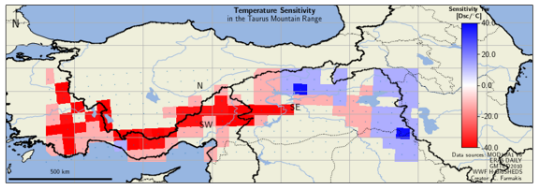

Table A.1: Comparison of the results (maps) for different ‘tile’ sizes, i.e., 30 km and 50 km. Average D_{SC} maps (column 1), Average rate of change of D_{SC} maps (column 2), Spatial coherence maps (column 3), Precipitation sensitivity maps (column 4), Temperature sensitivity maps (column 5)

Table A.1 compares the following maps for different ‘tile’ sizes:

1. Average D_{SC} maps (column 1),
2. Average rate of change of D_{SC} maps (column 2),
3. Spatial coherence maps (column 3),
4. Precipitation sensitivity maps (column 4),
5. Temperature sensitivity maps (column 5)

B

Appendix B

In the following chapter, the sensitivity of D_{SC} to inter-annual variability is examined using the second pair of climatic drivers.

The second two climatic drivers examined are the following:

1. The annual number of days with a mean temperature below zero.
2. The annual sum of precipitation on days when the temperature was below zero, which is a proxy for solid precipitation.

Figure B.1 illustrates the adjusted R-squared values estimated for the different climatic drivers. The purpose of computing the adjusted R-squared values is to get an idea of the explanatory powers of the following:

1. the annual number of days with a mean temperature below zero (D[Tw<0]) on D_{SC} (red boxes),
2. solid precipitation (Pw[Tw<0]) on D_{SC} (khaki boxes),
3. combined the aforementioned climatic drivers on D_{SC} (purple boxes).

The adjusted R-square was estimated using simple linear and multiple linear regression for each of the 100-m elevation bands in every sub-region.

Figure B.2 presents the sensitivities of D_{SC} to annual solid precipitation over the 2000-2019 period, for all elevation bands in every sub-region. Specifically, the figures show what the effect of a unit increase in annual solid precipitation would be on the annual number of snow cover days (D_{SC}).

Similarly, Figure B.3 illustrates the sensitivities of D_{SC} to annual solid precipitation over the 2000-2019 period, for all 'tiles' in TMR.

Figures B.4 and B.5 present the sensitivities of D_{SC} to the annual number of days with a temperature below zero over the 2000-2019 period, for all elevation bands in every sub-region (Figure B.4) and for all 'tiles' in TMR (Figure B.5).

Investigating the sensitivity of D_{SC} to inter-annual climatic variability using the number of days with temperature below zero and the annual solid precipitation results in the following conclusions:

- The annual number of days with a mean temperature below zero is an important driver in the South-West Taurus Mountains for elevations from 1500 m to 1800 m, e.g., an additional day with a mean temperature below zero would result in one more D_{SC} (see Figure B.4).
- In some regions on the Mediterranean coast of Turkey and in eastern TMR, an increase in the annual number of days with a mean temperature below zero would result in a decrease in D_{SC}, but in all other regions, an increase in the average winter temperature (Tw) would result in an increase in D_{SC} (see Figure B.5).
- Solid precipitation is important driver throughout TMR for elevations around 1500 m, e.g., 4 mm increase in annual solid precipitation would result in one more D_{SC} (see Figure B.2).

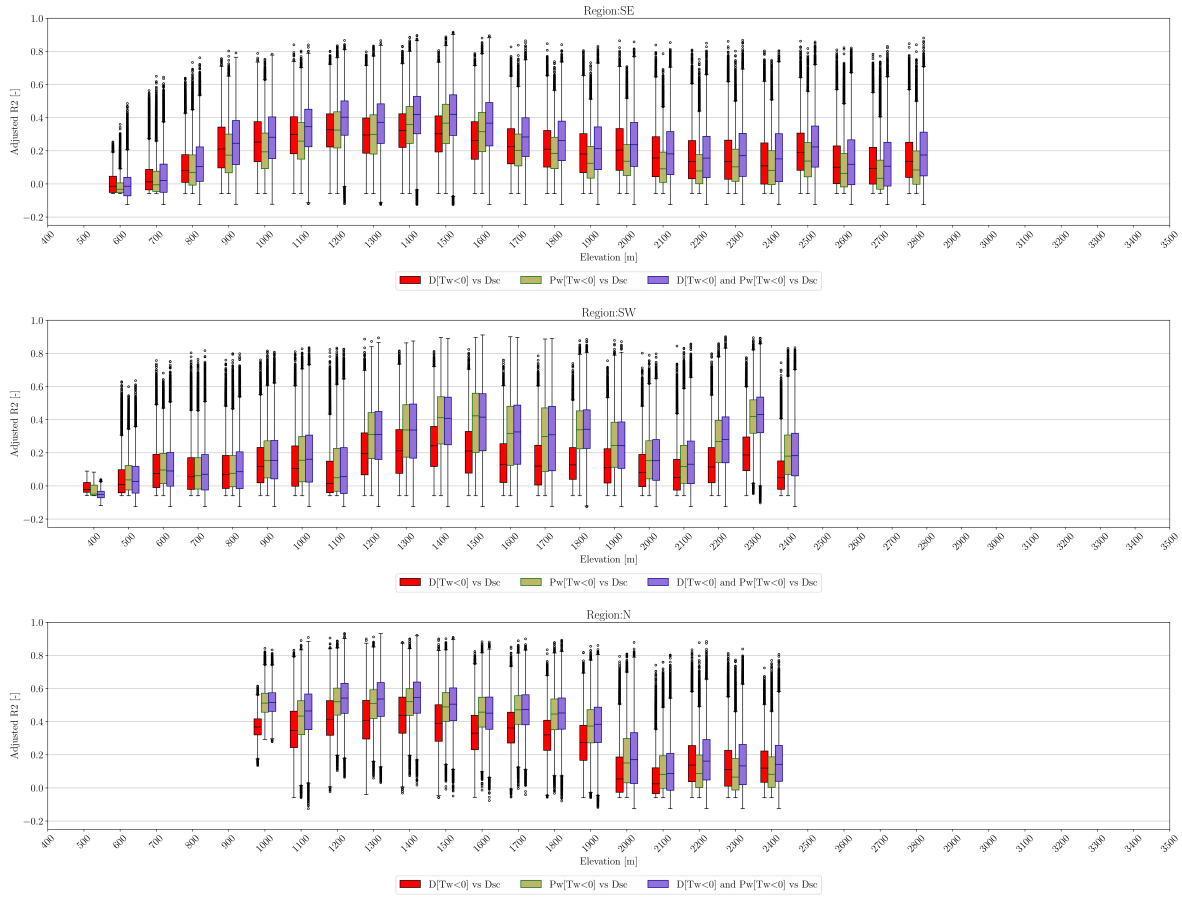

Figure B.1: Explanatory powers of the different climatic drivers, i.e., D[Tw<0] (red boxes), Pw[Tw<0] (khaki boxes) and both of them (purple boxes), using the adjusted R-square.

- In some regions on the Mediterranean coast of Turkey, an increase in annual solid precipitation would result in a decrease in D_{SC}, but in all other regions, an increase in solid precipitation would result in an increase in D_{SC} (see Figure B.3).

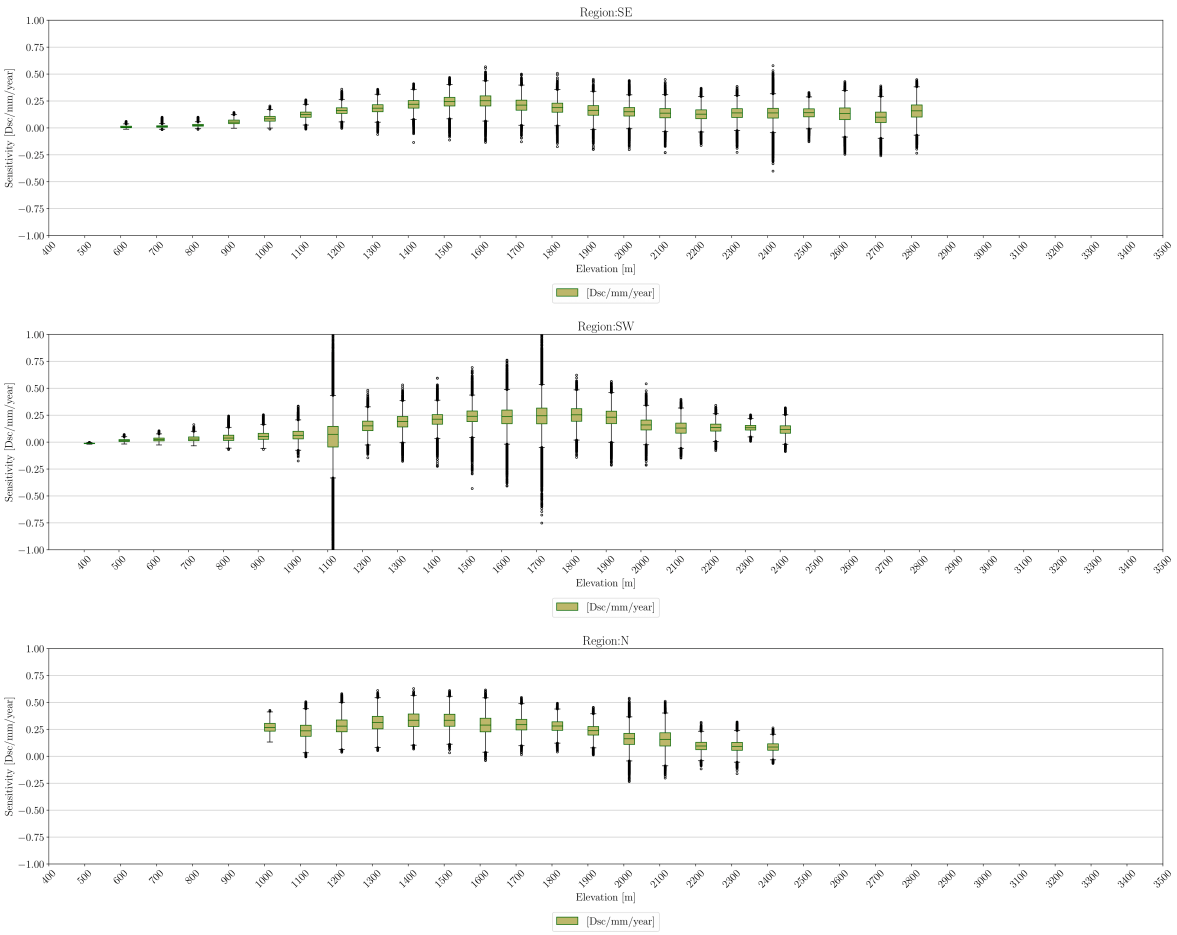

Figure B.2: Sensitivities of D_{SC} to annual solid precipitation, for all elevation bands in every sub-region.

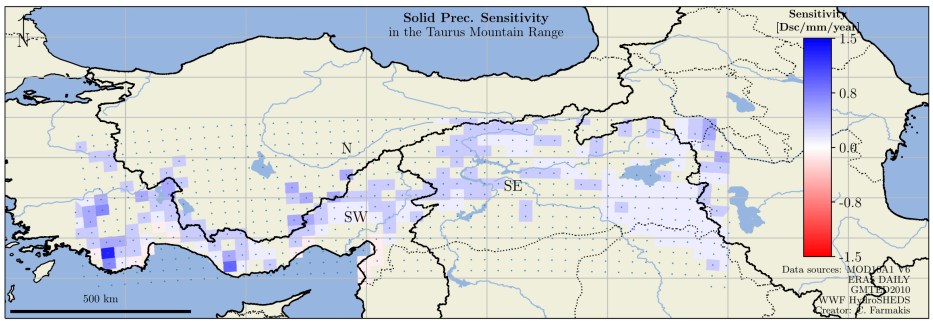

Figure B.3: Sensitivities of D_{SC} to annual solid precipitation, for all 'tiles' in TMR.

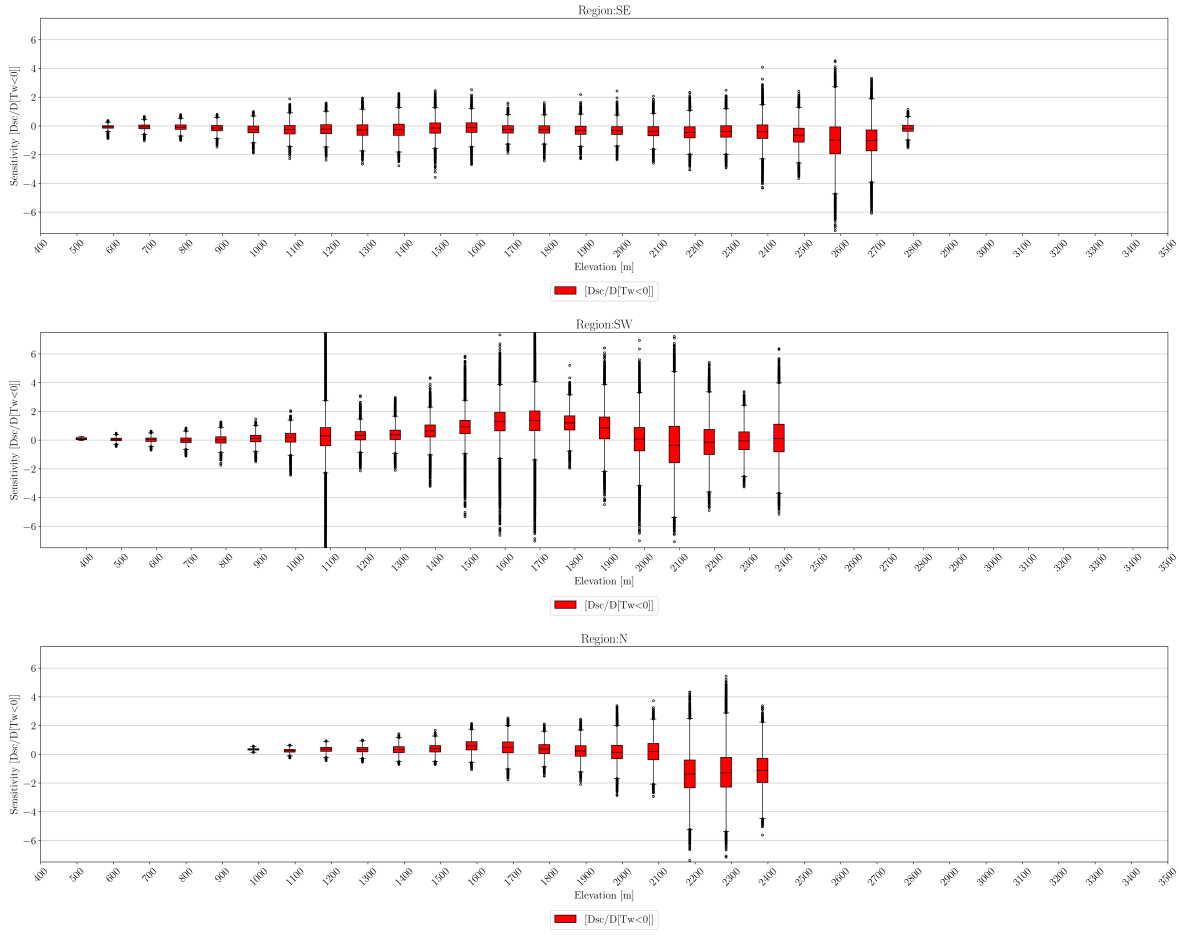

Figure B.4: Sensitivities of D_{SC} to the annual number of days with a mean temperature below zero (D[Tw<0]), for all elevation bands in every sub-region.

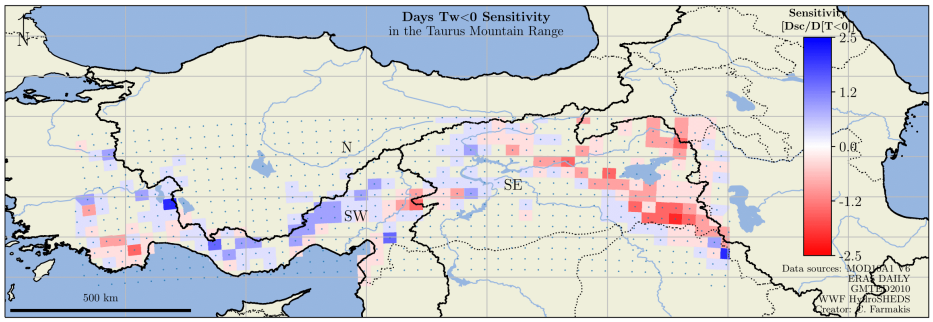

Figure B.5: Sensitivities of D_{SC} to the annual number of days with a mean temperature below zero (D[Tw<0]), for all 'tiles' in TMR.

C

Appendix C

The Google Earth Engine (GEE) script developed by van Esch (2019) [61]:

`https://code.earthengine.google.com/126da9f2dd0fdcad74b2e46ddc2994bd`

The Google Earth Engine (GEE) script developed by the author:

`https://code.earthengine.google.com/27f739de2402d5d6c435df6f81d2e376`

Additional information and scripts in GEE and/or Python can be provided by contacting the author of the present master thesis at the following email address:

chrysfarmakis@gmail.com